Chapter 7

Study of Nb addition on the microstructure, phase equilibria and oxidation behaviour of two Cr-Si based intermetallic alloys

7.1. Introduction

New high temperature Nb silicide alloys with capabilities beyond those Ni based super alloys will require coating system to operate in the environments of the next generation gas turbine engines [108]. Even though a coating system has not been identified to date, it is very likely that it will be of the bond coat (BC), thermally grown oxide (TGO), top coat type, often referred to as TBC system as described in the introduction of this thesis. The new coating system must be capable of forming in-situ alumina, silica or chromia oxides or mixture of these oxides as the TGO [6,109,111]. To design and develop oxidation resistant chromia, silica and alumina-forming BC alloys, it is essential to have comprehensive phase equilibria data, which is important for the optimization of alloy compositions and heat-treatment conditions [40]. Also for considering the effect of inter diffusion between BC and substrate on the long-term properties of both materials. This is particularly important for BCs on Nb silicide based alloy as diffusion of Nb from the substrate to the BC is expected. Protective scale formation remains a key challenge to the successful implementation of intermetallic alloys as BC alloys for structural application in high temperature environments. Furthermore, the knowledge of how alloy composition and its microstructure can be manipulated to influence the oxidation response of intermetallic is a key factor to design and develop coating systems.

To date, there have been some investigations of phase equilibria in the Cr-Si-Al and Cr-Si-Nb systems [10,40,51,52,124,140-148]. We have already discussed previous work on the Cr-Si-Al system in chapter 5 and 6. The motivation for this work was to study the microstructures and oxidation resistance of the Cr-45Si-5Al-5Nb (AN5) and Cr-25Si-25Al-5Nb (AN6) alloys and understand how the Nb addition affects microstructure development, phase stability and oxidation behaviour of Cr-Si-Al-Nb alloys with different Si/Al ratios. This is important because as was the case for the alloys AN1, AN2, AN3 and AN4 diffusion of Nb from the substrate is expected during service and we wish to know how Nb effects the microstructure and oxidation of Al poor and Al rich Cr-Si-Al alloys (in the case of alloys AN1 and AN2 the diffusing species from the substrate is Hf and AN3 and AN4 alloys is Ti as discussed in section 5.1 and 6.1).

7.2. Results

7.2.1 The microstructure of the alloys AN5 and AN6

The phases present in the as-cast and heat treated alloy AN5 were the orthorhombic V_6Si_5-type Nb_6Si_5 (OI44), the tetragonal W_5Si_3-type Cr_5Si_3 and the hexagonal $CrSi_2$-type $CrSi_2$ whereas the orthorhombic V_6Si_5-type Nb_6Si_5 (OI44) and $Nb_{11}Si_8$ (OP76), tetragonal W_5Si_3-type Cr_5Si_3 and hexagonal Mn_5Si_3 -type Nb_5Si_3 intermetallics together with the rhombohedral Cr_5Al_8–type Cr_5Al_8, cubic Cu_5Zn_8-type Cr_4Al_9 were formed in the alloy AN6 In this chapter, the Cr_5Si_3 and Nb_5Si_3 with Nb, Cr and Si in solid solution is referred to as $(Cr,Nb)_5(Si,Al)_3$ and $(Nb,Cr)_5(Si,Al)_3$ and the $CrSi_2$ with Al in solid solution as $Cr(Si,Al)_2$. The Nb_6Si_5 and $Nb_{11}Si_8$ with Al and Cr in solid solution are referred to as $(Nb,Cr)_6(Si,Al)_5$ and $(Nb,Cr)_{11}(Si,Al)_8$, respectively. Likewise, the Cr_5Al_8, Cr_4Al_9 with Si in solid solution are referred to as $Cr_5(Al,Si)_8$ and $Cr_4(Al,Si)_9$, respectively.

7.2.1.1 As cast Cr-45Si-5Al-5Nb (alloy AN5-AC)

The volume fractions of the phases formed in the microstructure of the alloy AN5 are given in the Table 7-1. The microstructure of AN5-AC consisted of 41.1% Nb_6Si_5, 28.6 % Cr_5Si_3 and 30.3 % $CrSi_2$, Table 7-1. The data in the Table 7-2 summarizes the compositions of the phases in the bulk (centre) of the button ingot. Compared with the nominal composition, the actual composition of AN5-AC was very close to it. According to the XRD data (Figure 7.1), EBSD data and BSE images (Figure 7.2) and the EDX data (Table 7-2), the Nb_6Si_5, Cr_5Si_3 and $CrSi_2$ phases were present in the microstructure of AN5-AC. In the Figure 7.2 (b) the dark contrast phase is the $CrSi_2$, the grey contrast phase is the Cr_5Si_3 and the bright contrast phase is the Nb_6Si_5. The growth direction of columnar Nb_6Si_5 and Cr_5Si_3 silicides was perpendicular to the button ingot surface, the Cr_5Si_3 was formed either adjacent to the 6-5 silicide or was surrounded by $CrSi_2$. In the Nb_6Si_5 silicide there was no solubility of Al and the maximum solubility of Nb was 13.6 at.%. Therefore, the stoichiometry of the 6-5 silicide was $Nb_{1.5}Cr_{4.5}Si_5$. In the Cr_5Si_3, the Nb and Al solubilities were in the ranges 0.4 to 1.2 and 0.7 to 1.1 at.%. In the $CrSi_2$ desilicide, there was no solubility of Nb and the solubility of Al was 13.2 at.%.

7.2.1.2 Heat treated Cr-45Si-5Al-5Nb (alloy AN5-HT)

The alloy was given two different heat treatments, namely 1200 ^{o}C/100 h, 1300 ^{o}C/100 h. The actual composition of alloy the heat-treated at 1200 ^{o} C was Cr-44.1Si-4.2 Nb-5.5 Al, close to the nominal alloy composition, see Table 7-2.

According to the XRD data (Figure 7.1) and the EDX data (Table 7-2), the heat-treated microstructure at 1200 ^{o}C consisted of the same silicides, namely the Nb_6Si_5, Cr_5Si_3 and $CrSi_2$. Typical backscatter electron images of AN5-HT1200 are shown in Figure 7.2 c and d. The actual composition of the specimen heat treated at 1300 ^{o}C was Cr-43.0Si-5.2Nb-5.0Al, slightly leaner in Si. Considering the XRD data (Figure 7.1) and the EDX data (Table 7-2) the Nb_6Si_5, Cr_5Si_3 and $CrSi_2$ silicides were still present in the microstructure of AN5-HT1300, with vol. % essentially the same as after the heat treatment at 1200 ^{o}C, see Table 7-1.

Table 7-1 Density and data for % areas of constituent phases in the as cast (AC) and heat treated (HT) alloys AN5 and AN6

Alloy [a]	**Density (g/cm^3)**	**Nb_6Si_5/$Nb_{11}Si_8$ (%)**	**Cr_5Si_3 /Nb_5Si_3 (%)**	**$CrSi_2$ (%)**	**Al_8Cr_5 (%)**	**Al_9Cr_4 (%)**
AN5-AC	5.48±0.02	41.1/0	28.6/0	30.3	-	-
AN5-HT1200	-	33.4/0	39.1/0	27.4	-	-
AN5-HT1300	-	32.9/0	39.5/0	27.5	-	-
AN6-AC	5.11±0.01	20.1/13.2	30.2/0	-	33.5	3.1
AN6-HT1200	-	-	49.1/5.2	-	(21.2+24.5[b])	-
AN6-HT1300	-	-	49.8/7.8	-	34.2[+]	4.2
AN6-HT13[c]	-	-	12.7/45.1	-	39.7[+]	-

a AC=as cast , HT1200 = heat treatment at 1200 °C/100 h, HT1300 = heat treatment at 1300 °C /100 h. b 24.5 % is the volume fraction of Nb rich Al8Cr5. c different area in the centre of the ingot. + In AN6-HT13 and AN6-HT13c, there was porosity, respectively of 3.7 and 2.5%.

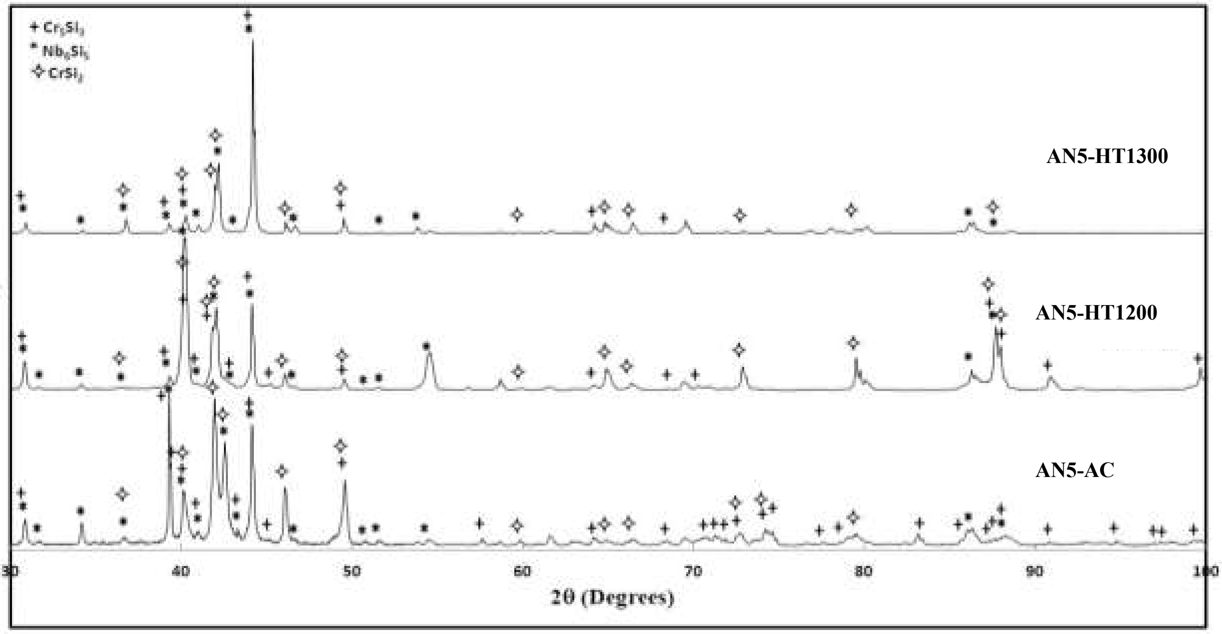

Figure 7.1 X-ray diffractograms of the as cast and heat treated alloy AN5 (card number: 01-089-4866 for $CrSi_2$, 00-050-1329 for Cr_5Si_3 and 04-007-7466 for Nb_6Si_5) (HT1200 = heat treatment at 1200 ^oC/100h, HT1300 = heat treatment at 1300 ^oC /100h)

The phases in the microstructure of the alloy AN5 were remarkably stable. Indeed, the in Cr_5Si_3 (HT1200) phase the Si+Al concentration was ~ 39.1 at.% with Al/Si ≈ 0.03 and in the $CrSi_2$ (HT1200), the Si+Al concentration was ~ 66.2 at.% with Al/Si ≈ 0.27. In the Cr_5Si_3 (HT1300) phase, the Si+Al concentration was ~ 37.7 at.% with Al/Si ≈ 0.04 and in the $CrSi_2$ (HT1300), the Si+Al concentration was ~ 65.1 at.% with Al/Si ≈ 0.27. Compared with the cast alloy, the volume fraction of the Cr_5Si_3 increased after the heat treatment at 1200 ^oC and did not change at 1300 ^oC. The volume fraction of the $CrSi_2$ was slightly reduced after the heat treatment at 1200 ^oC and did not change at 1300 ^oC. The same was the case for the Nb_6Si_5 phase.

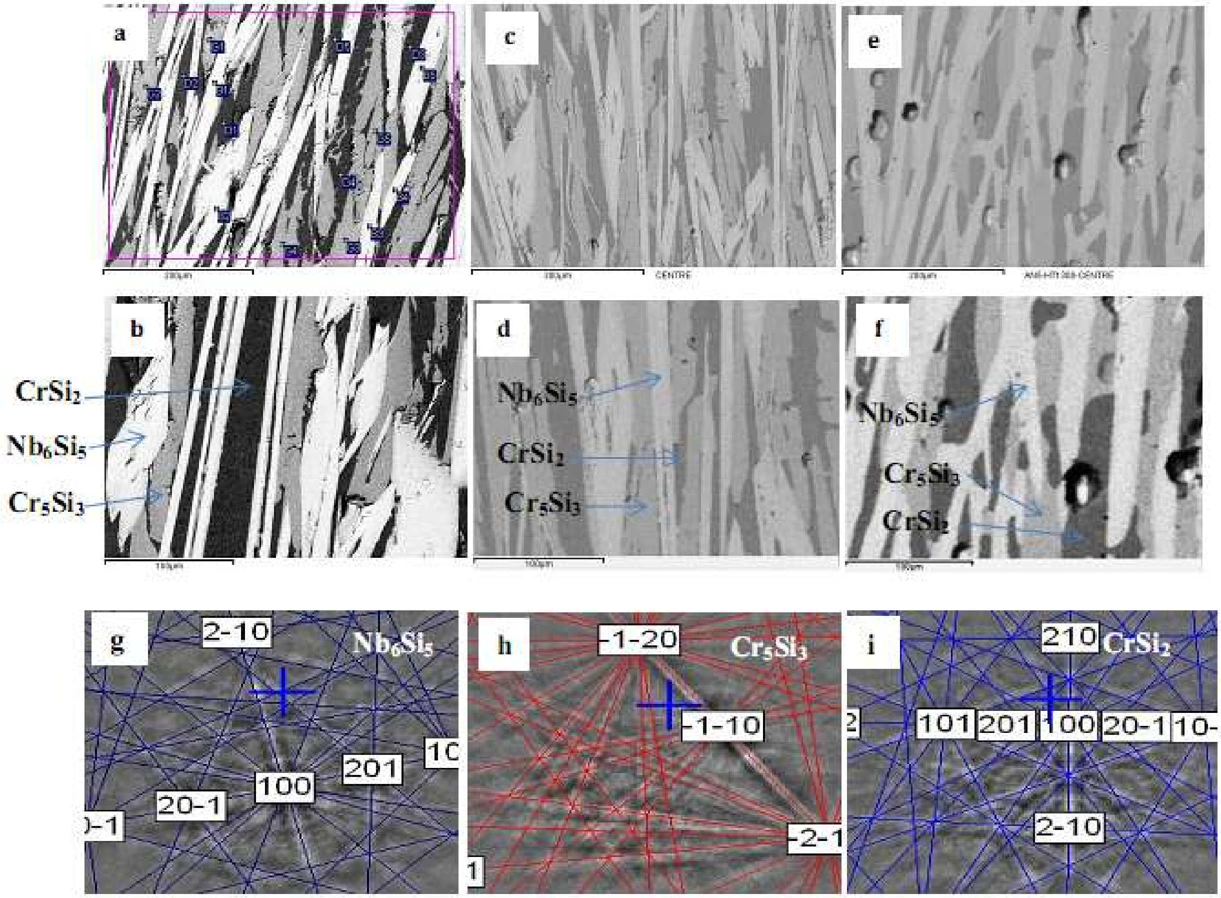

Figure 7.2 Microstructure of the alloy AN5 a,b) as-cast c,d) Heat-treated at 1200 ° C for 100 h e,f) Heat-treated at 1300 ° C for 100 h and g, h, i) EBSD patterns of phases, where (g) is for the Nb_6Si_5, (h) is for the Cr_5Si_3 and (i) is for the $CrSi_2$.

Table 7-2 Quantitative EDX analysis (at. %) data of the as cast (AC) and heat treated (HT b) alloy AN5

Phase	Cr	Si	Nb	Al
AN5-AC[a,b]	43.1±0.3	45.6±0.3	5.9±0.5	5.8±0.5
	42.6-43.4	45.3-45.8	5.7-6.4	5.3-6.3
$(Nb,Cr)_6Si_5$	41.3±0.2	45.3±0.2	13.4±0.3	-
	41.1-41.5	45.1-45.5	13.2-13.6	-
$(Cr,Nb)_5(Si,Al)_3$	59.3±0.2	39.1±0.3	0.8±0.4	0.9±0.2
	59.1-59.5	38.7-39.5	0.4-1.2	0.7-1.1
$Cr(Si,Al)_2$	33.4±0.5	53.1±1.6	-	13.2±1.8
	32.9-33.8	51.5-54.8	-	11.4-15.1
AN5-HT1200[a,b]	46.2±0.8	44.1±1.1	4.2±0.6	5.5±0.7
	45.5-47.0	43.0-45.2	3.7-4.8	4.8-6.2
$(Nb,Cr)_6Si_5$	41.9±0.8	44.1±0.8	13.6±0.9	-
	41.1-42.7	43.3-44.9	12.7-14.6	-
$(Cr,Nb)_5(Si,Al)_3$	60.2±0.5	37.9±0.2	1.2±0.1	1.2±0.2
	59.7-60.7	37.7-38.1	1.1-1.3	1.0-1.5
$Cr(Si,Al)_2$	33.9±0.3	52.1±0.4	-	14.1±0.1
	33.7-34.2	51.7-52.4	-	14.0-14.2
AN5-HT1300[a,b]	47.0±0.1	43.0±0.2	5.2±0.3	5.0±0.2
	46.9-47.1	42.8-43.2	4.9-5.4	4.8-5.1
$(Nb,Cr)_6Si_5$	45.5±1.6	44.1±0.2	10.3±1.9	-
	43.9-47.2	43.9-44.3	8.5-12.2	-
$(Cr,Nb)_5(Si,Al)_3$	62.1±0.7	36.1±0.2	-	1.6±0.1
	61.4-62.7	35.9-36.3	-	1.5-1.7
$Cr(Si,Al)_2$	34.7±1.2	51.2±0.6	-	13.9±0.4
	33.5-35.8	50.6-51.8	-	13.5-14.2

[a] Large area analysis from the center of the button

[b] AC=as cast , HT1200 = heat treatment at 1200 °C/100 h, HT1300 = heat treatment at 1300 °C /100 h.

7.2.1.3 As cast Cr-25Si-25Al-5Nb (alloy AN6-AC)

The microstructure of the button ingot and the phases in AN6-AC are given in Figure 7.3 to 7.5 and Table7-3. The data in the latter summarizes the compositions of the phases in the bulk of the button. The composition of AN6-AC was very close to the nominal composition of the alloy. According to the XRD (Figure 7.3) and EDX data (Table7-3) for AN6-AC, the Nb_6Si_5, $Nb_{11}Si_8$, Cr_5Si_3, Cr_5Al_8 and Cr_4Al_9 phases were present in the microstructure of the cast alloy. There was also Nb rich Nb_6Si_5 where the phase contrast was brighter than that of Nb_6Si_5. The EBSD technique was used to aid phase identification in the alloy and confirm the crystal structures of the phases. The EBSD maps of each phase are shown in the Figure 7.5. The MAD values were between 0.1-0.5 in the pattern matching process provided by Chanel 5 software (see section 4.6.1) In the AN6-AC, the growth direction of needle-shape Nb_6Si_5 silicides was either perpendicular or diagonal to the surface of round shape Cr_5Si_3 that was formed adjacent to the $Nb_{11}Si_8$ silicide. The coarse plate-shape bright contrast phase was the 11-8 silicide that was surrounded by the Cr_5Si_3 in some areas. Thin plates of the Nb_6Si_5 silicide were surrounded by Al_8Cr_5 and Al_9Cr_4 aluminides. The solubility of Al in $Nb_{11}Si_8$ was about 4.7 at.% and the maximum solubility of Nb was 13.7 at.%. In the Nb_6Si_5 silicide, the Al and Nb

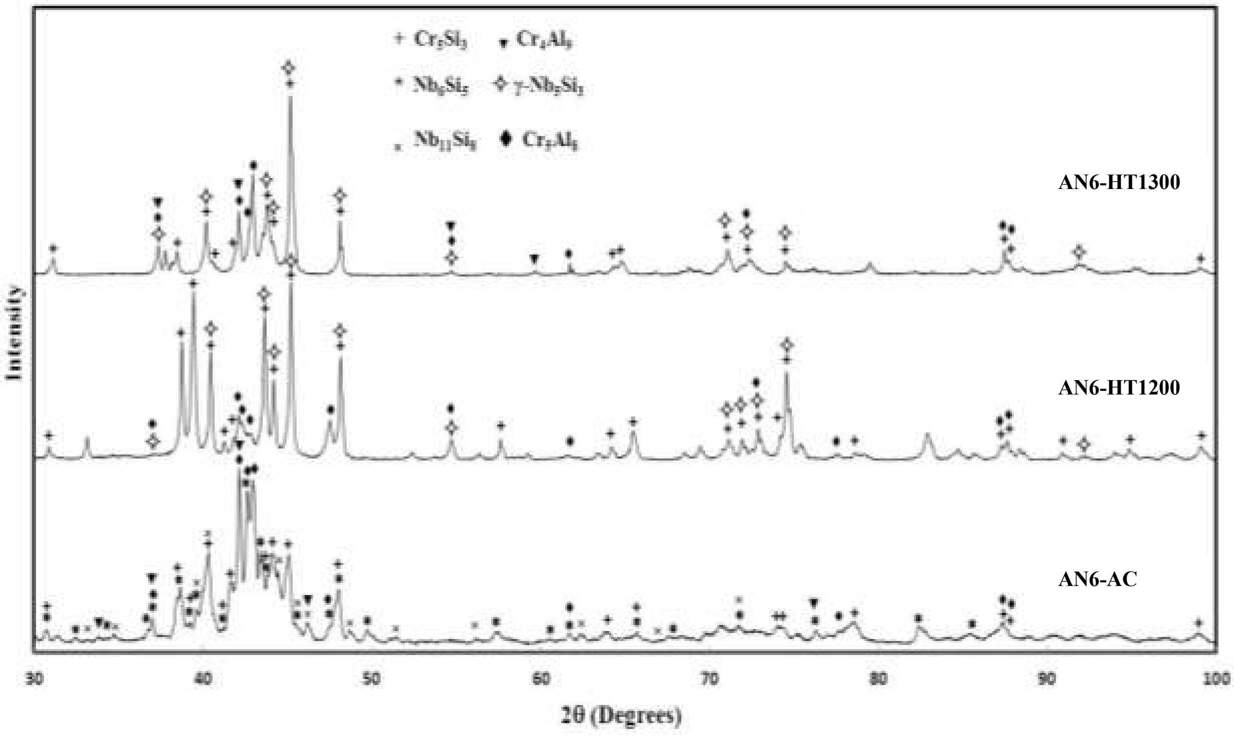

Figure 7.3 X-ray diffractograms of the as cast and heat treated alloy AN6(card number 00-050-1329 for Cr_5Si_3, 00-008-0422 for γ Nb_5Si_3, 04-007-7466 for Nb_6Si_5, 00-002-1192 for Cr_5Al_8, 00-034-0432 for $Nb_{11}Si_8$ and 00-002-1193 for Cr_4Al_9) (HT1200 = heat treatment at 1200 °C/100h, HT1300 = heat treatment at 1300 ° C /100h).

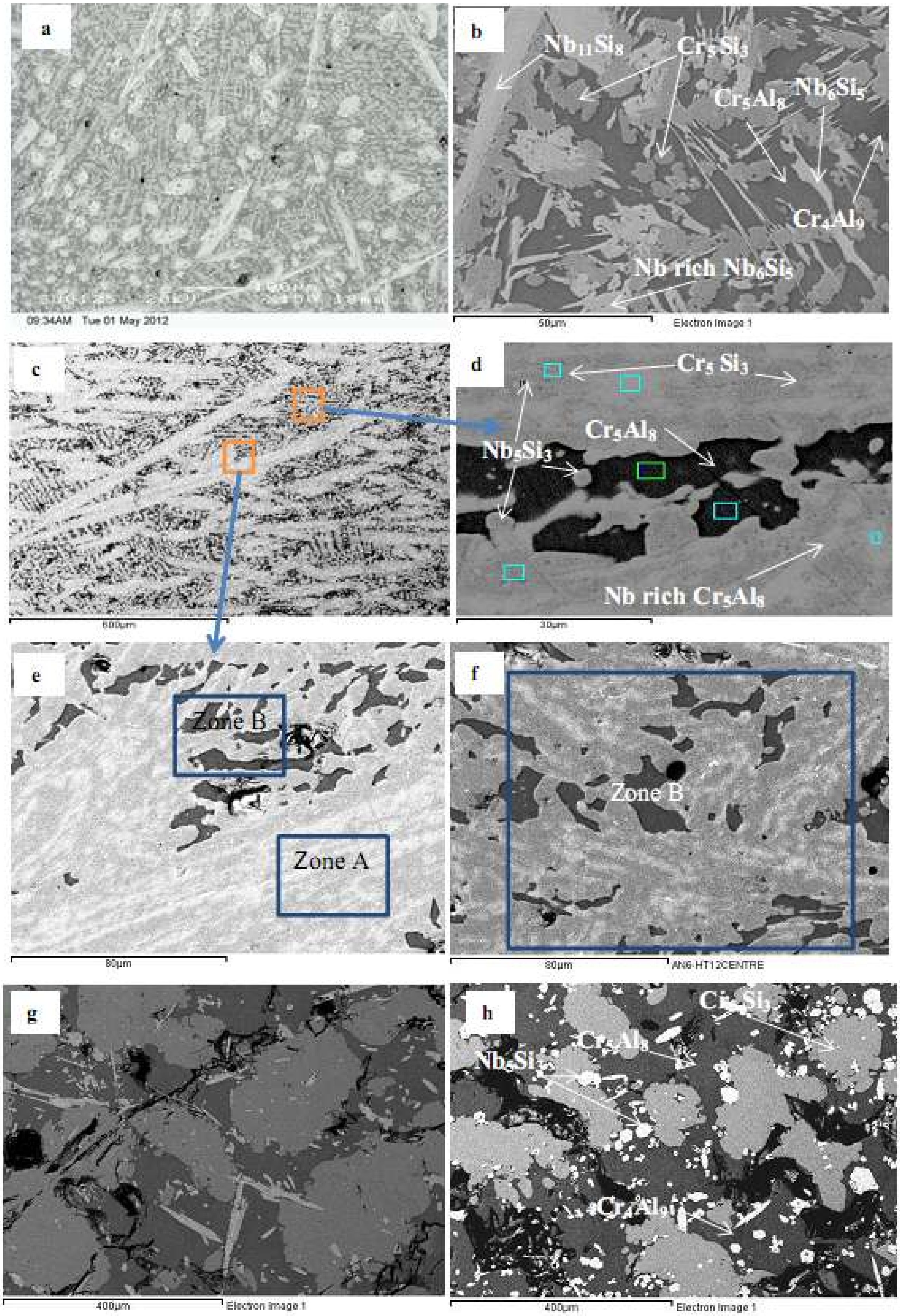
a
09:34AM Tue 01 May 2012
b
$Nb_{11}Si_8$
Cr_5Si_3
Cr_5Al_8
Nb_6Si_5
Cr_4Al_9
Nb rich Nb_6Si_5
50µm
Electron Image 1
c
600µm
d
Cr_5 Si_3
Cr_5Al_8
Nb_5Si_3
Nb rich Cr_5Al_8
30µm
e
Zone B
Zone A
80µm
f
Zone B
80µm
AN6-HT12CENTRE
g
400µm
Electron Image 1
h
Cr_5Si_3
Cr_5Al_8
Nb_5Si_3
Cr_4Al_9
400µm
Electron Image 1

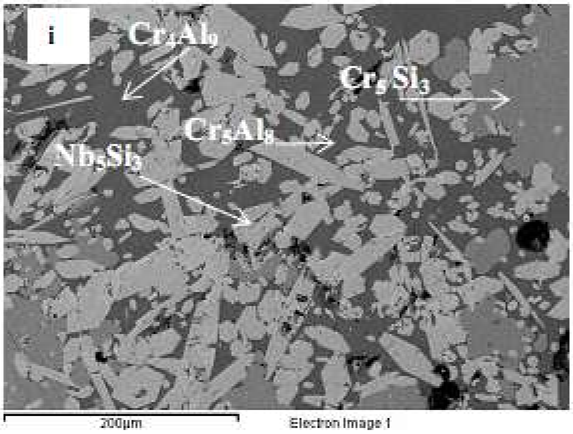

Figure 7.4 Microstructure of alloy AN6 a, b) as-cast condition c, d, e,f) Heat-treated at 1200 ° C and g, h, i) Heat-treated at 1300 ° C for 100 h.

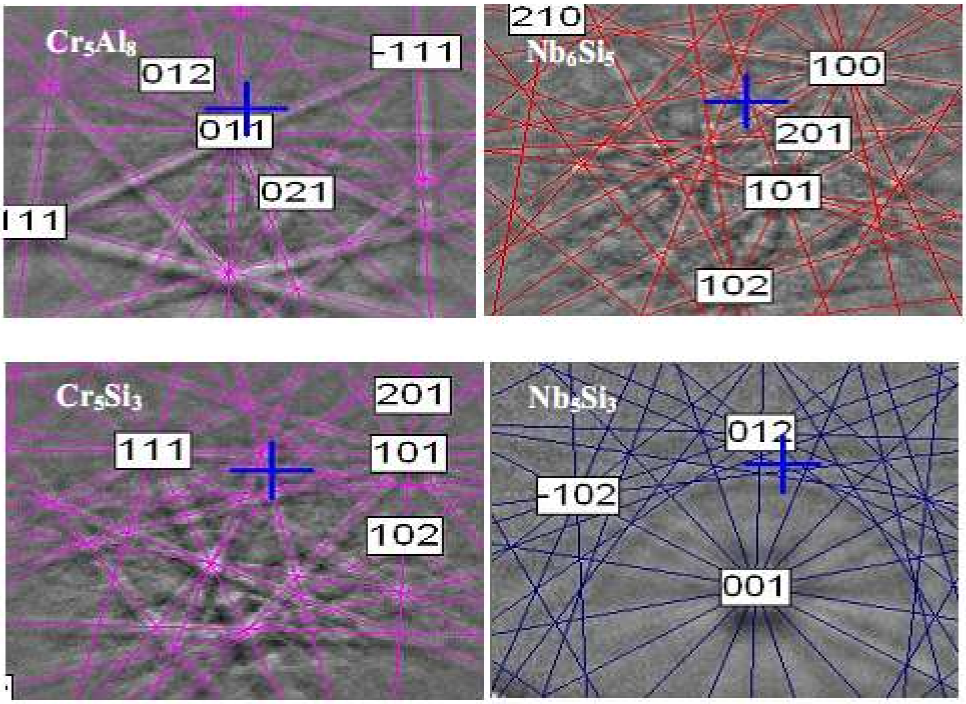

Figure 7.5 EBSD patterns of the phases in the alloy AN6.

Table 7-3 Quantitative EDX analysis (at. %) data of the as cast and heat treated alloy AN6

Phase	Cr	Si	Nb	Al
AN6-AC[a,b]	44.6±1.2	26.1±0.9	4.8±0.9	24.6±0.5
	43.4-45.8	25.2-27.0	3.9-5.6	24.1-25.2
$(Nb,Cr)_{11}(Si,Al)_8$	44.6±0.7	37.5±0.9	13.2±0.5	4.7±0.9
	43.9-45.3	36.6-38.4	12.7-13.7	3.7-5.6
$(Nb,Cr)_6(Si,Al)_5$[c]	40.2±0.6	39.40±0.5	14.4±0.3	5.5±0.4
	39.6-40.9	38.90-39.80	14.1-14.8	5.1-5.9
$(Nb,Cr)_6(Si,Al)_5$	45.7±0.9	37.6±0.6	9.5±0.7	6.1±0.5
	44.8-46.6	37.0-38.2	8.8-10.2	5.6-6.6
$(Cr,Nb)_5(Si,Al)_3$	58.6±0.7	36.1±0.9	3.1±0.4	2.2±0.8
	57.9-59.3	35.2-37.1	2.7-3.5	1.5-3.0
$Cr_5(Si,Al)_8(\gamma_{\text{-H}})$	36.3±0.7	8.7±0.9	0.7±0.2	54.4±1.1
	35.6-37.0	7.8-9.6	0.5-0.9	53.4-55.5
$Cr_4(Si,Al)_9(\tau_4)$	30.1±0.6	11.9±0.9	0.5±0.3	57.8±1.6
	29.5-30.7	11.0-12.8	0.2-0.8	56.2-59.4
AN6-HT1200[a,b]	42.7±0.6	24.2±0.4	5.2±0.3	27.9±0.2
	42.1-43.3	23.8-24.6	4.9-5.5	27.7-28.1
$Cr_5(Si,Al)_3$	61.6±0.2	36.7±0.2	-	1.8±0.2
	61.4-61.8	36.5-36.9	-	1.6-2.1
$(Nb,Cr)_5(Si,Al)_3$[d]	51.0±0.6	35.7±0.8	11.4±0.5	1.8±0.3
	50.4-51.6	34.9-36.5	10.9-11.9	1.5-2.1
$Cr_5(Si,Al)_8$	34.9±0.4	6.7±0.2	-	58.5±0.3
	34.5-35.3	6.5-6.9	-	58.2-58.8
$(Nb,Cr)_5(Si,Al)_8(\gamma_{\text{-H}})$	15.6±1.8	4.7±1.8	17.7±0.9	62.3±2.2
	13.8-17.3	2.9-6.4	16.8-18.7	60.1-64.6
Zone A[+]	37.3±1.1	22.8±0.8	8.4±0.6	31.5±1.2
	36.2-38.4	22.0-33.6	7.8-9.0	30.3-32.7
Zone B[+]	32.6±1.5	22.0±0.8	3.8±0.2	41.6±0.9
	31.1-34.1	21.2-22.8	3.6-4.0	40.7-42.5
AN6-HT1300[a,b]	45.4±0.7	26.1±0.9	2.0±0.2	26.6±1.6
	44.7-46.2	25.2-26.9	1.8-2.2	25.0-28.2
$(Cr,Nb)_5(Si,Al)_3$	60.4±0.5	36.6±0.6	1.0±0.2	2.1±0.3
	59.9-60.9	36.0-37.2	0.8-1.2	1.8-2.4
$(Nb,Cr)_5(Si,Al)_3$[d]	44.7±0.8	35.7±0.2	17.0±0.8	2.7±0.3
	43.9-45.5	35.5-35.9	16.2-17.8	2.4-2.9
$Cr_5(Si,Al)_8(\gamma_{\text{-H}})$	34.7±0.3	8.1±0.4	-	57.4±0.9
	34.4-35.0	7.7-8.5	-	56.5-58.2
$Cr_4(Si,Al)_9(\tau_4)$	29.8±0.5	10.3±0.5	0.6±0.1	59.3±1.1
	29.3-30.3	9.8-10.8	0.5-0.7	58.2-60.4

[a] Large area analysis from the center of the button [b]AC=as cast , HT1200 = heat treatment at 1200 °C/100 h, HT1300 = heat treatment at 1300 °C/100 h.

[c] Nb-rich $(Nb,Cr)_6Si_5$ phase [+] see text section 7.2.1.4

[d] Given that the XRD suggested the presence of Mn_5Si_3 type 5-3 silicide, it is proposed that the Nb rich Cr_5Si_3 was Mn_5Si_3-type $(Nb,Cr)_5Si_3$ (γNb_5Si_3)

solubilities were 6.1 at.% and 9.5 at.% but in the Nb rich Nb_6Si_5 the Nb content increased to 14.4 at.%. The Al and Nb solubilities in Cr_5Si_3 were low, 2.2 at.% and 3.1 at.%, respectively. There were also Cr rich areas in the microstructure, see Figure 7.4 (b) (bright contrast area adjacent to Cr_5Si_3 phase). The brighter and darker contrast areas were Al_8Cr_5 and Al_9Cr_4, respectively. The microstructure of AN6-AC consisted of 33.3 % Nb_6Si_5 + $Nb_{11}Si_8$ silicides, 30.2 % 5-3 Cr silicide and 36.6 % aluminides (Table 7-1).

7.2.1.4 Heat treated Cr-25Si-25Al-5Nb (alloy AN6-HT)

The alloy was given two different heat treatment at 1200 ^{o}C/100h and 1300 ^{o}C/100h. The actual composition of the specimen heat-treated at 1200 ^{o} C was Cr-24.2Si-27.9Al-5.2 Nb. Compared with the nominal composition the alloy was richer in Al. According to the XRD (Figure 7.3) and the EDX (Table 7-3) data, the microstructure of AN6-HT1200 consisted of two phases, namely the 5-3 silicide and Al_8Cr_5 aluminide with strong partitioning of Nb in them. The aforementioned phases were found in two areas that exhibited different microstructure. There are identified as zone A and zone B in Table 7-3 and differ in their Al and Nb contents with zone A being richer in Nb and poorer in Al compared with zone B. The significant microstructure change in AN6-HT1200 was attributed to the occurrence of incipient melting in the alloy at 1200^{o}C. The DSC trace (Figure 7.6) also indicated melting below 1200 ^{o}C. The melting reaction was attributed to the τ_4 phase as the Cr_4Al_9 aluminide melts at about 1170 ^{o}C according to the Al-Cr binary system, see Figure 2.2. The Nb_6Si_5 and $Nb_{11}Si_8$ that were present in AN6-AC were not observed in AN6-HT1200 and instead Nb rich Cr_5Si_3 was formed. It is suggested that the latter was the hexagonal Mn_5Si_3 type Nb_5Si_3. This phase was present at volume fraction less than 6 % compared with the high volume fraction (~49%) of the Cr_5Si_3. In the zones A and B the bright contrast phase was the Nb rich Al_8Cr_5 and the grey contrast phase was the Al_8Cr_5.

After the heat treatment at 1300 ^{o}C, the actual composition of AN6-HT1300 was Cr-26.1Si-26.6Al-2.0Nb, and was poorer in Nb compared with the nominal concentration. According to the XRD and EDX data (Figure 7.4 and Table 7-3), the Cr_5Si_3, Nb_5Si_3, Al_8Cr_5 and Al_9Cr_4 phases were present in the microstructure. The coarsening of the microstructure was attributed to incipient melting of the alloy during the heat treatment. However, compared with AN6-HT1200, the τ_4 re-formed during the solidification of the liquid in some parts of the microstructure. The

Nb rich 5-3 silicide was present with low and high vol.% in different areas of the alloy. This phase is suggested to be the Mn_5Si_3 type Nb_5Si_3. In some areas of the microstructure, the solubility of Al in the 5-3 silicides was in the range 2-3 at.%, in agreement with other work [144]. In the Cr_5Al_8 the solubility of Si was around 8 at.%. The 5-3 silicides and the $Cr_5(Al,Si)_8$ were the dominant phases in the microstructure, see Table 7-1.

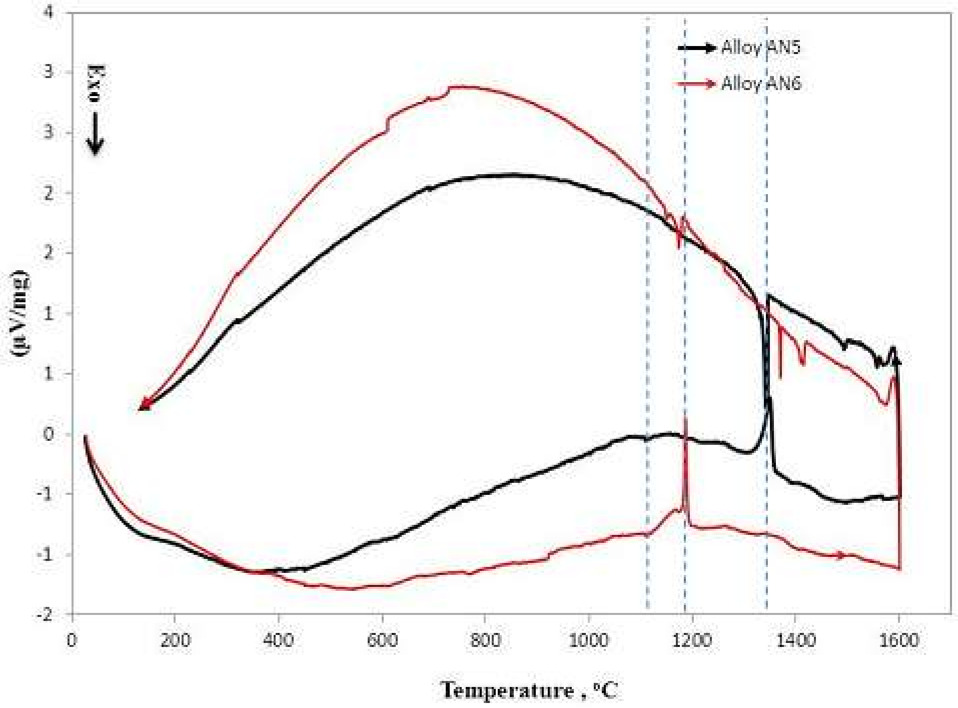

Figure 7.6 DSC traces of the alloys AN5 and AN6 obtained at 20 $Kmin^{-1}$ heating rate in flowing Argon

7.2.2 Isothermal oxidation of the as cast alloys AN5 and AN6

Oxidation experiments were performed at 800, 1000 and 1200 °C, as described in chapter 3. Oxidation kinetics data and the morphology of the oxide scales are presented in the following sections. For the oxidation kinetics, see also the Appendix A.

7.2.2.1 Oxidation kinetics

Figure 7.7 shows the weight changes of the alloys versus time at the three temperatures and Figure 7.8 shows the oxidation kinetics of the alloys as a function of time. The Figure 7.8 (a) shows that parabolic, near parabolic and cube kinetics were exhibited by the alloy AN5 that showed partial parabolic oxidation behaviour after 1000 min at 800 ^{o}C. This alloy followed a near linear behaviour during the first 1000 min of exposure where the oxidation rate exponent (n) was 0.68. At 1000 ^{o}C the alloy showed cube kinetic (n=0.31) for the first 26 h of oxidation and this was followed by low oxidation (n= 0.08) that would suggest the formation of protective scale on the surface. At 1200 ^{o}C, the alloy AN5 followed parabolic oxidation for t <1000 min exposure time and this was succeeded by low oxidation (n=0.10).Thus, the alloy AN5 exhibited remarkable oxidation after 1000 min exposure at each temperature. In the alloy AN6 the weight gain at 1000 ^{o}C and 1200 ^{o}C was lower than that at 800 ^{o}C and more reduction was seen at 1000 ^{o}C. Figure 7.8 (b) shows the isothermal oxidation kinetics of the alloy AN6 for the three temperatures. The alloy followed near parabolic oxidation behaviour as the oxidation rate exponent n was close to 0.5 at 800, 1000 and 1200 ^{o}C, see Table 7-4. The parabolic oxidation rate constants were $6.6\mathrm{x}10^{-8}$, $5.9\mathrm{x}10^{-9}$ and $1.6\mathrm{x}10^{-8}$ g^2/cm^4s, respectively at 800, 1000 and 1200 ^{o}C.

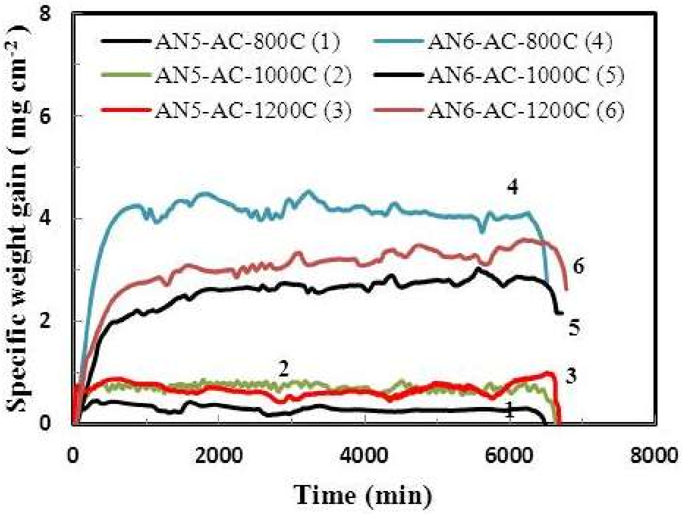

Figure 7.7 Weight changes of the alloys AN5 and AN6 after isothermal oxidation in air at 800, 1000 and 1200 ^{o}C.

This alloy (AN6) showed liquation at the heat treatment at 1200 °C. Yet, it had the lower k_p value at 1200 °C. The liquation was caused by the melting of the τ_4 phase, but the vol.% of this phase is very low in AN6-AC (~3%), see Table 7-1 and its distribution was not uniform. Therefore, it is highly likely that the cube specimen of AN6 oxidized at 1200 °C might have had no τ_4. If this is correct then we would deduce that the τ_4 phase is not desirable.

Table 7-4 Total weight gains, oxidation rate constants and oxidation rate exponents of the alloys AN5 and AN6 at 800, 1000 and 1200 °C

Alloy	**Weight gain (mg/cm2)**	**kp (g2.cm-4.s-1)**	**kc (g3.cm-6.s-1)**	**n**
AN5-800 °C	0.29	1.7 x10-13 (t > 16 h)	-	0.5465
AN5-1000 °C	0.67		2.0x10-12(t < 16 h)	0.314
AN5-1200 °C	0.95	7.2x10-12 (t < 16 h)	-	0.5522
AN6-800 °C	4.11	6.6 x10-8 (t =100 h)	-	0.4806
AN6-1000 °C	2.84	5.9 x10-9 (t =100 h)	-	0.4754
AN6-1200 °C	3.54	1.6 x10-8 (t =100 h)	-	0.4575

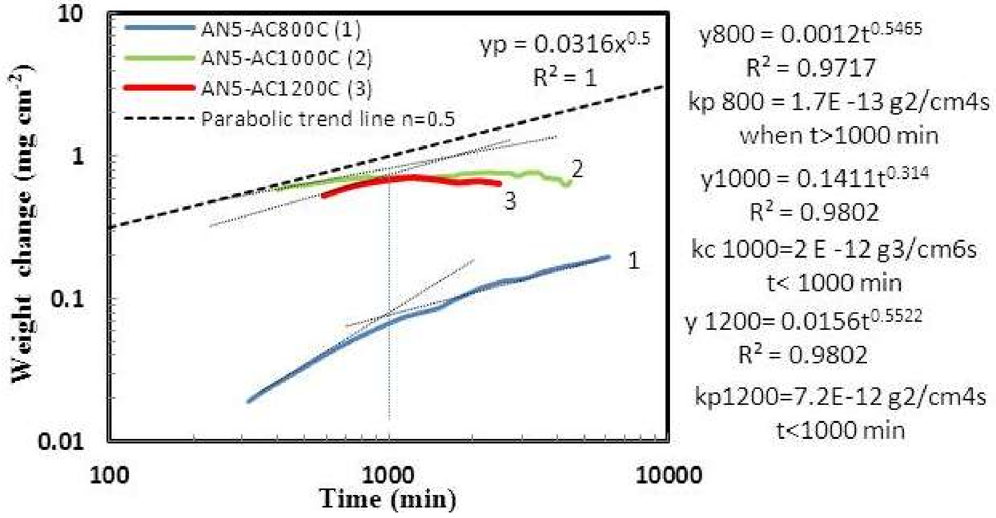

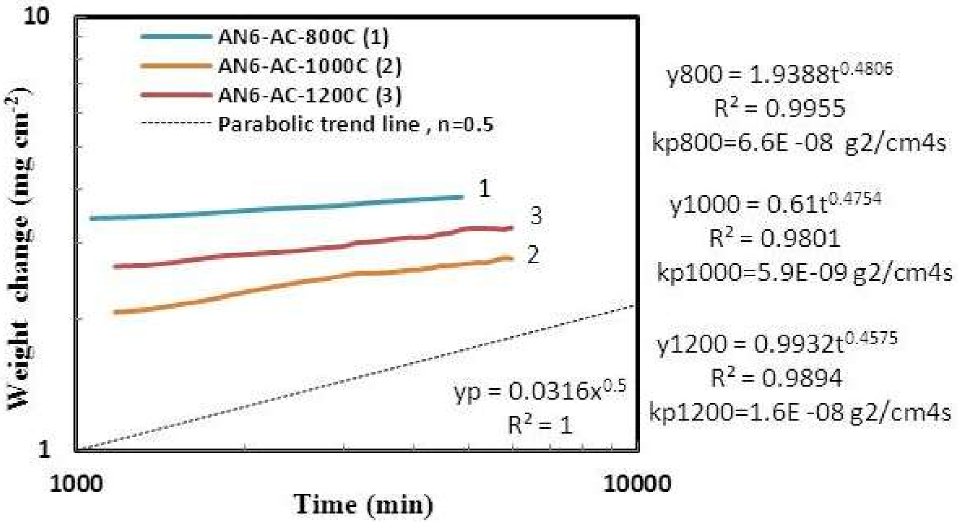

Figure 7.8 The log-log plots of weight change versus exposure time for a) the AN5 and b) AN6 alloys at 800, 1000 and 1200 °C. Dotted lines correspond to parabolic kinetics, (n=0.5)

Considering the n values, it is concluded that the alloys AN5 and AN6 followed near parabolic oxidation kinetics with the exception of the alloy AN5 at 1000 °C which showed cube oxidation kinetics at $t < 16$ h.

Figure 7.8 (a, b) shows that in general, the n value was close to 0.5 or less for the alloy AN5 and AN6 in the temperature range 800 to 1200 °C. The parabolic oxidation rate constants of the alloys AN5 and AN6 at the three temperatures were plotted in the Arrhenius-type plot in Figure 7.9.

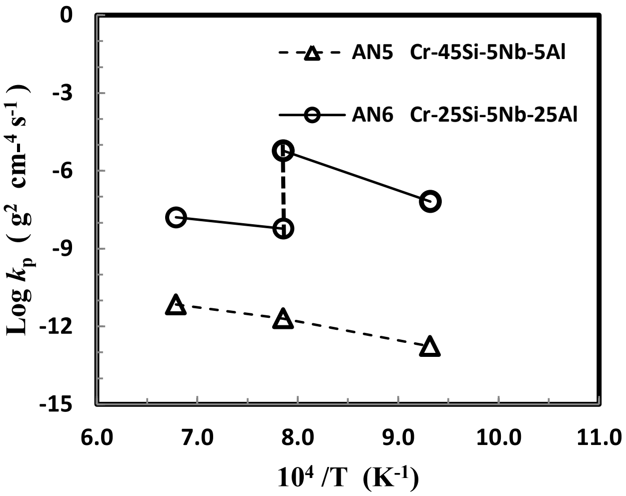

Figure 7.9 Arrhenius plots of the parabolic oxidation rate constants versus reciprocal temperature for the alloys AN5 and AN6.

The activation energies for oxidation were obtained from the slopes of the linearly fitted data, the equation 1 [112].

$$k_p = k_0 . \exp(-Q_A/RT) \qquad \text{Equation 1}$$

where k_p is the parabolic oxidation rate constant ($g^2cm^{-4}s^{-1}$), k_0 is the pre-exponential factor, R is the gas constant (8.3144 J/Kmol), T is the absolute temperature (Kelvin) and Q_A is the activation energy of the overall oxidation reaction (kJ/mol). The activation energy of oxidation for the alloy AN5 was 122.1 kJ/mol in the temperature range 800 to 1200 °C and for the alloy AN6, it was 261.5 and 77.8 kJ/mol, respectively for the ranges 800 to 1000 °C and 1000 to 1200 °C. The former value is close to the activation energy for alumina formation in NiAl aluminde given by Grabke et al. [149].

Table 7-5 Activation energies for the growth of oxidation of the alloys AN5 and AN6.

Alloy	(Temperature range °C)	Activation energy ($kJmol^{-1}$)
AN5-AC	800-1200	122.1±2.3
AN6-AC	800-1000	261.5± 3.5
AN6-AC	1000-1200	77.8±2.7

Figure 7.9 shows that a single mechanism was operative in the entire temperature range of oxidation of the alloy AN5. Figure 7.9 would suggest that the oxidation mechanism of the alloy AN6 was changed at 1000 °C. The activation energy for oxidation of the alloy AN6 at 800-1000 °C was approximately 3.4 times higher than that at 1000-1200 °C. This indicated that the alloy AN6 potentially possessed better oxidation above 1000 °C.

7.2.2.2 Oxide scale characterization

Secondary electron micrographs of the surfaces of oxidized as-cast AN5 and AN6 specimens are shown respectively in Figures 7.10 and 7.11 for the temperatures 800, 1000 and 1200 °C. The glancing angle XRD data is shown in Figures 7.12 and 7.13 for the alloys AN5 and AN6 for the three-oxidation temperatures.

At 800 °C the alloy AN5 formed a mixture of oxides consisting of non-uniform alumina oxide (Figure 7.12 a) along with patches of silica scale where there was Nb_2O_5 oxide formed on the surface of facetted silicon-rich intermetallics. The growth rates of the oxides were different due to the different activation energies of oxide formation on each precursor phase. The cube specimen of AN5 retained clear edges after oxidation at 800 °C, see right hand edge of cube specimen in Figure 7.10 a1. The Figure 7.10 a2 and a4 show the growth of dense rough alumina in the scale with an uneven surface where the alumina formed on $CrSi_2$ with higher growth rate compared with oxides formed on Cr_5Si_3 (dark contrast, Figure 7.10 a2). The Figure 7.10 a3 and a5 respectively show a patch of cellular silica and Nb_2O_5 fine grain oxide particles formed on the surface of Nb_6Si_5 silicide precursors in the microstructure of the alloy.

At 1000 °C, a mixture of alumina, silica and chromia formed on the surface of the alloy AN5 (Figure 7.12 b). The cube specimen retained clear edges after oxidation at 1000 °C, see Figure 7.10 b1. The scale was non-uniform and thickened with growth of alumina flakes on the surface that consisted of button shape ridge multi facet grains (Figure 7.10 b3 and b4). In some areas where the silica formed (Figure 7.10 b2 and 7.13_1), the morphology of the scale changed to equiaxed fine microstructure of silica which seemed not to be as dense as the alumina scale.

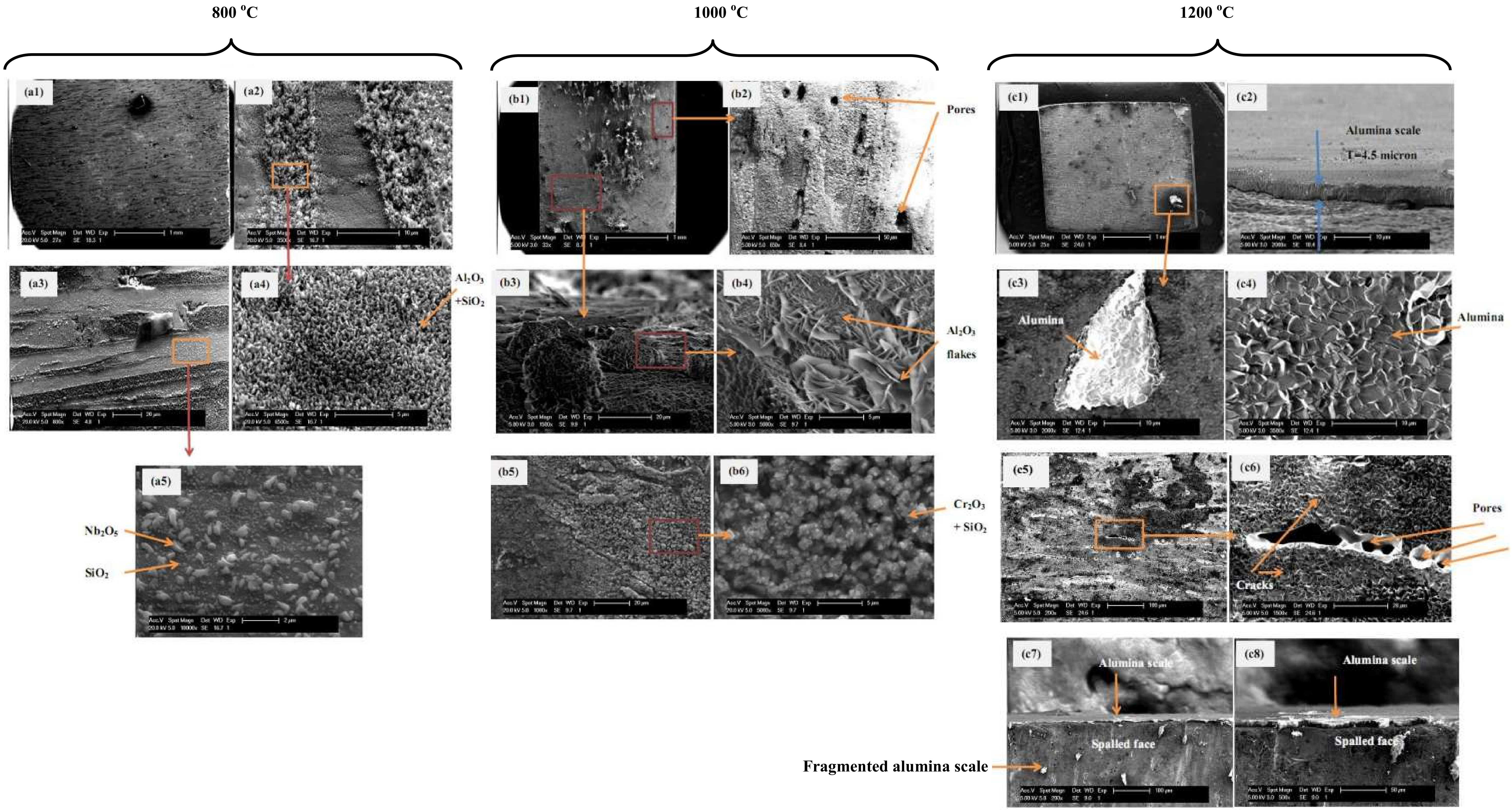

Figure 7.10 SEM-SE images of oxide scales formed on the AN5 alloy after 100 h oxidation in air at (a1 to a6) 800 ^{o}C, (b1 to b6) 1000 ^{o}C and (c1 to c8) 1200 ^{o}C.

There were also pores in the scale, see Figure 7.10 b2. Pores would have formed due to the depletion of Cr, Si and Al by outward diffusion during oxidation. According to the glancing angle XRD data (Figure 7.12 b) the most dominant oxide at 1000 ^{o}C was alumina. The growth of chromia and silica oxides, as the secondary oxide species, was patchy in the outer surface of the scale.

At 1200 ^{o}C there was formation of uniform thin alumina scale (Figure 7.10 c2 and c8 and Figure 7.12 c) which possessed rather good adherence to the substrate (Figure 7.10 c2) in the two faces of the specimen. This was attributed to the lower thermal expansion miss-match of alumina oxide with the multi-phase substrate. The cube specimen of AN5 retained clear edges after oxidation at 1200 ^{o}C, see Figure 7.10 c1.The thickness of the uniform alumina scale was about 4.5 μm. In some areas, the scale had spalled entirely, while in others a macro crack was formed (Figure 7.10 c6) probably during cooling of the specimen to the ambient temperature. Voids were also observed; see Figure 7.10 c5 and c6. The voids beneath the alumina scale were formed because of depletion of Al by outward diffusion to the surface to form protective scale. However, the distribution and morphology of voids was not the same as that seen at 1000 ^{o}C. The EDX data of the alumina scale formed at 1200 ^{o}C showed that it contained 0.3-1.7 at.% and 0.5-1.7 at.% respectively of Si and Cr. The $CrSi_2$ had the highest Al concentration of all the phases present in the substrate (Table 7.2) and therefore was the main supplier of Al during the oxidation of the alloy at each temperature.

Secondary electron images of the oxidation samples of the alloy AN6 are shown in Figure 7.11 and the glancing angle XRD data is shown in Figure 7.13. At 800 ^{o}C, the alloy formed almost a uniform alumina oxide scale on the surface of the specimen with patches of either chromia, silica or mixture of silica and alumina, see Figure 7.11 a1-a6 and Figure 7.13 a.

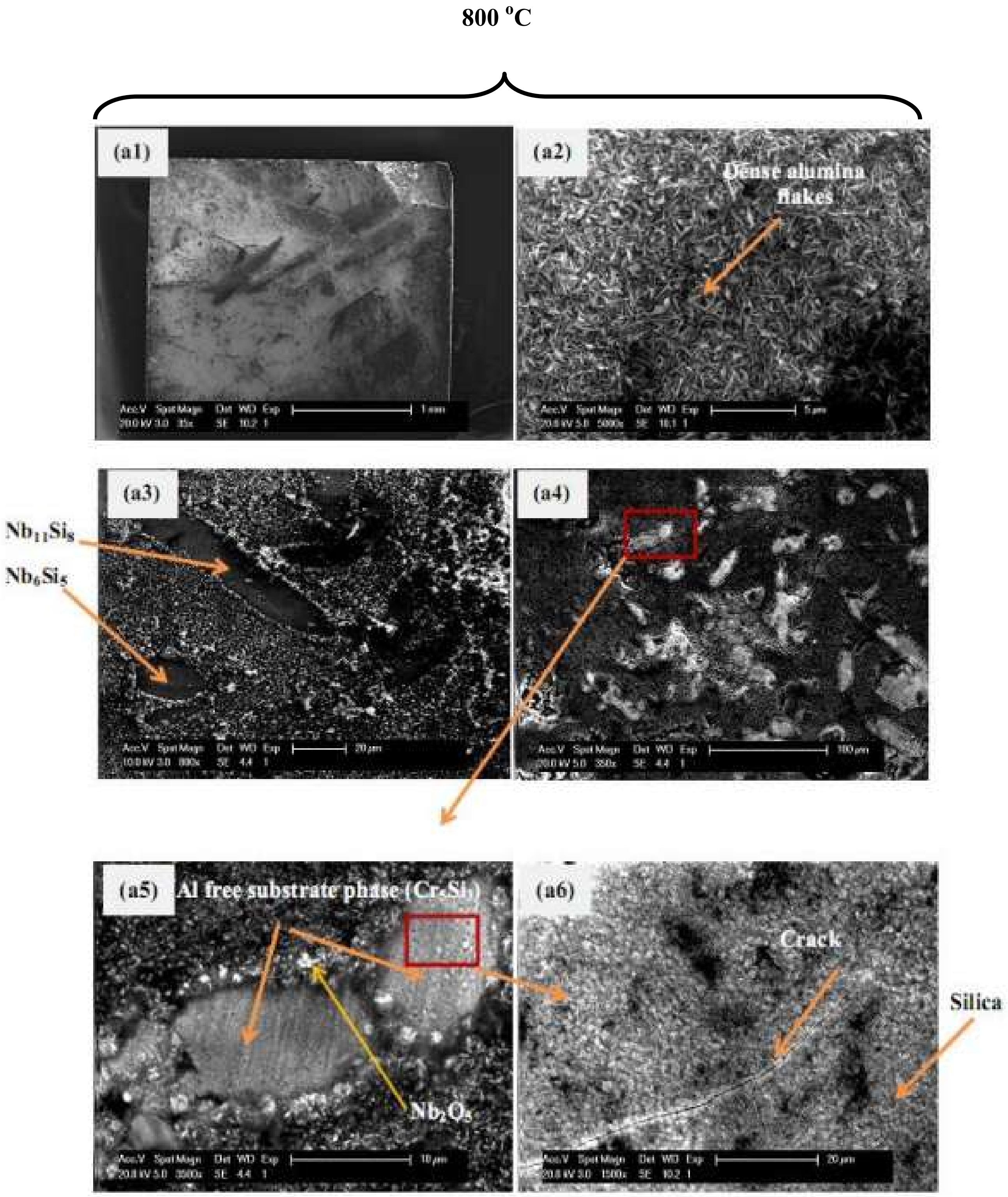

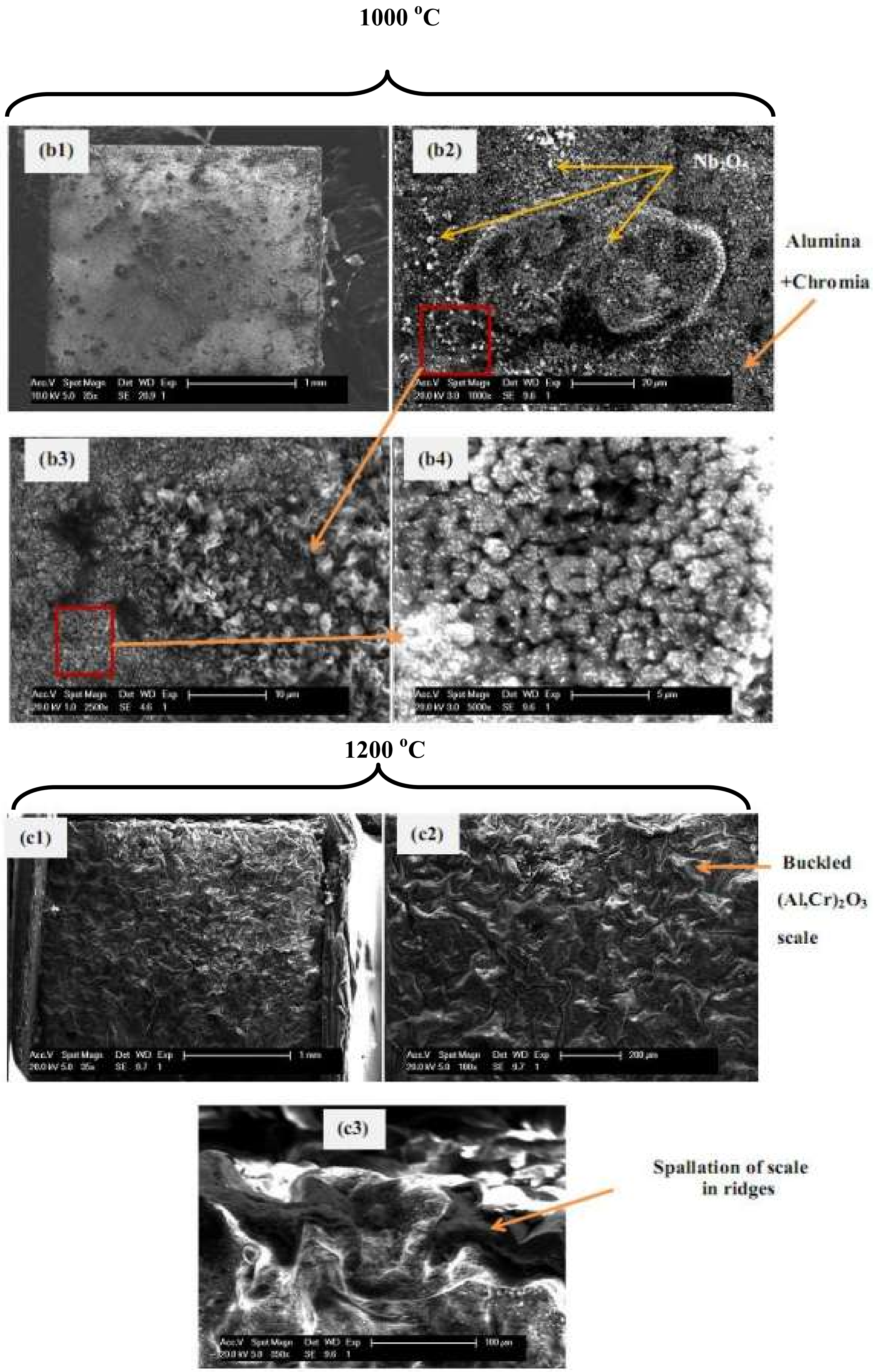

Figure 7.11 SEM-SE images of oxide scales formed on the as cast AN6 alloy after 100 h oxidation in air at (a1 to a4) 800 °C, (b1 to b6) 1000 °C and (c1 to c3) 1200 °C.

Figure 7.11 a2 shows alumina flakes adjacent to the silica and chromia patches. According to the cross section studies, there was no evidence of sub scale formation on the surface at 800 °C. In Figure 7.11 a3 and a4, the chromia and silica patches are shown by the bright and grey contrasts on the surface of the specimen. It is suggested that silica and chromia were formed on either of the Cr_5Si_3 or Nb_6Si_5 silicide precursors. The phase exhibiting bright contrast in the Figure 7.11 a4 was chromia oxide that was surrounded by alumina oxide.

At 1000 °C the scale consisted of uniform alumina oxide together with patches of Nb_2O_5 and chromia oxide, see Figure 7.13 b. The bright area in Figure 7.11 b2 corresponds to Nb_2O_5 oxide where the polygonal grain grown on the surface is chromia. The scale was quite smooth and its outer surface was not convoluted. The scale was very adherent to the substrate and there was no evidence of any spallation between substrate and scale.

At 1200 ° C, as shown in Figure 7.11 (c1-c6), the scale was highly corrugated due to the lateral growth of alumina that was attributed to the multi directional outward diffusion of aluminium to the surface. The outer scale was alumina (Figure 7.13 c) and the scale was of uniform thickness but it had spalled and broken on the ridge which might be owing to the thermal expansion mismatch between substrate and oxide scale. The cracks on the scale could also be attributed to the formation of wrinkles on the scale that caused residual stress on the scale and led to a crack and rupture in the surface of the specimen. At this temperature, as mentioned above the scale was of uniform thickness without any spallation except in some areas on the ridges where spallation occurred (see Figure 7.11 c3). Figure 7.11 c4 shows that the scale had highly rough surface, which was not observed at the lower oxidation temperatures. This suggests that due to the strong adherence of the scale to the substrate, the growth and thermal stresses were relieved by substrate deformation. The second important conclusion is that in later stages of the reaction, void and subsequently cracks began to form in the scale. Through these physical defects, oxygen may penetrate into the scale, contributing to the overall scale growth. Therefore, the parabolic oxidation rate constant of the alloy was increased to $1.6\text{x}\ 10^{-8}\ g^2cm^{-4}s^{-1}$ at 1200 °C, compared with that at 1000 °C which was $5.9\text{x}10^{-9}\ g^2cm^{-4}s^{-1}$.

(a)

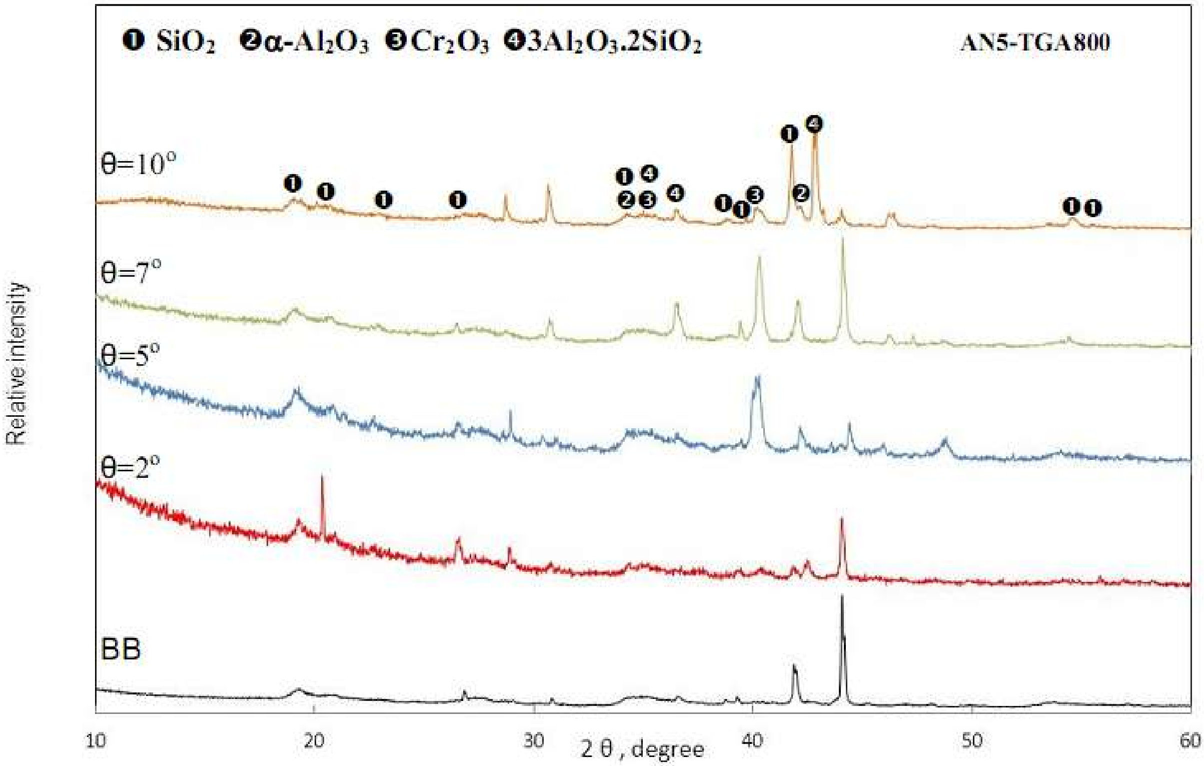
❶ SiO_2 ❷α-Al_2O_3 ❸Cr_2O_3 ❹$3Al_2O_3.2SiO_2$
AN5-TGA800
θ=10°
θ=7°
θ=5°
θ=2°
BB
Relative intensity
2 θ , degree
10
20
30
40
50
60

(b)

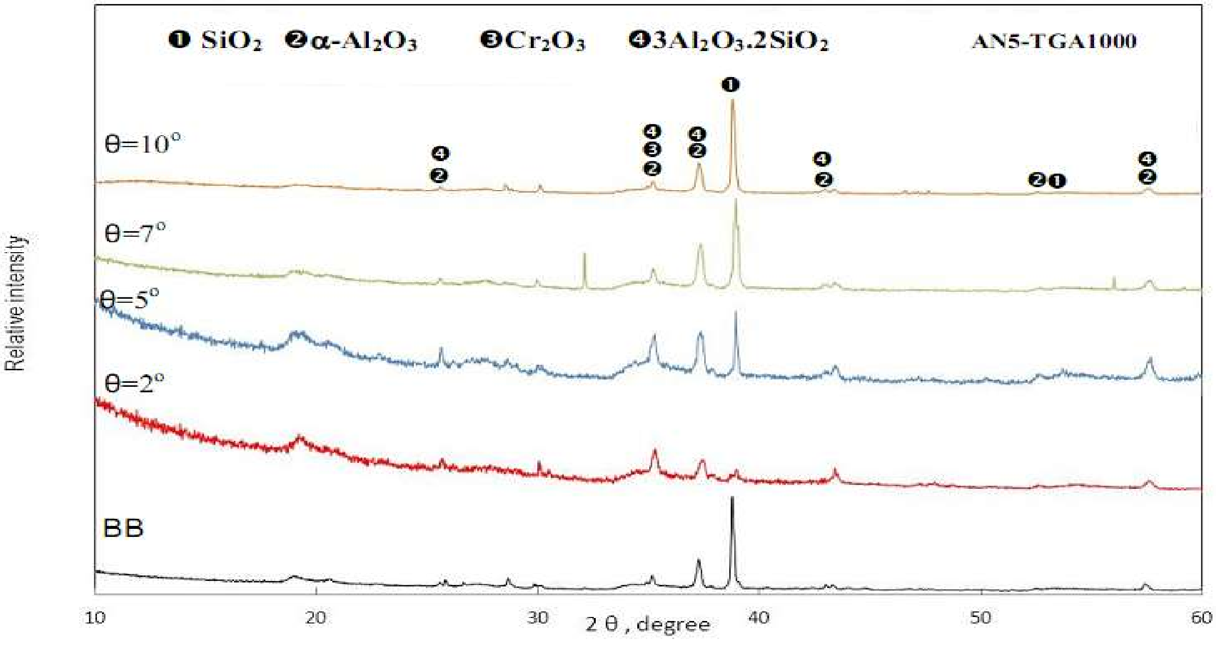
❶ SiO_2 ❷α-Al_2O_3 ❸Cr_2O_3 ❹$3Al_2O_3.2SiO_2$
AN5-TGA1000
θ=10°
θ=7°
θ=5°
θ=2°
BB
Relative intensity
2 θ , degree
10
20
30
40
50
60

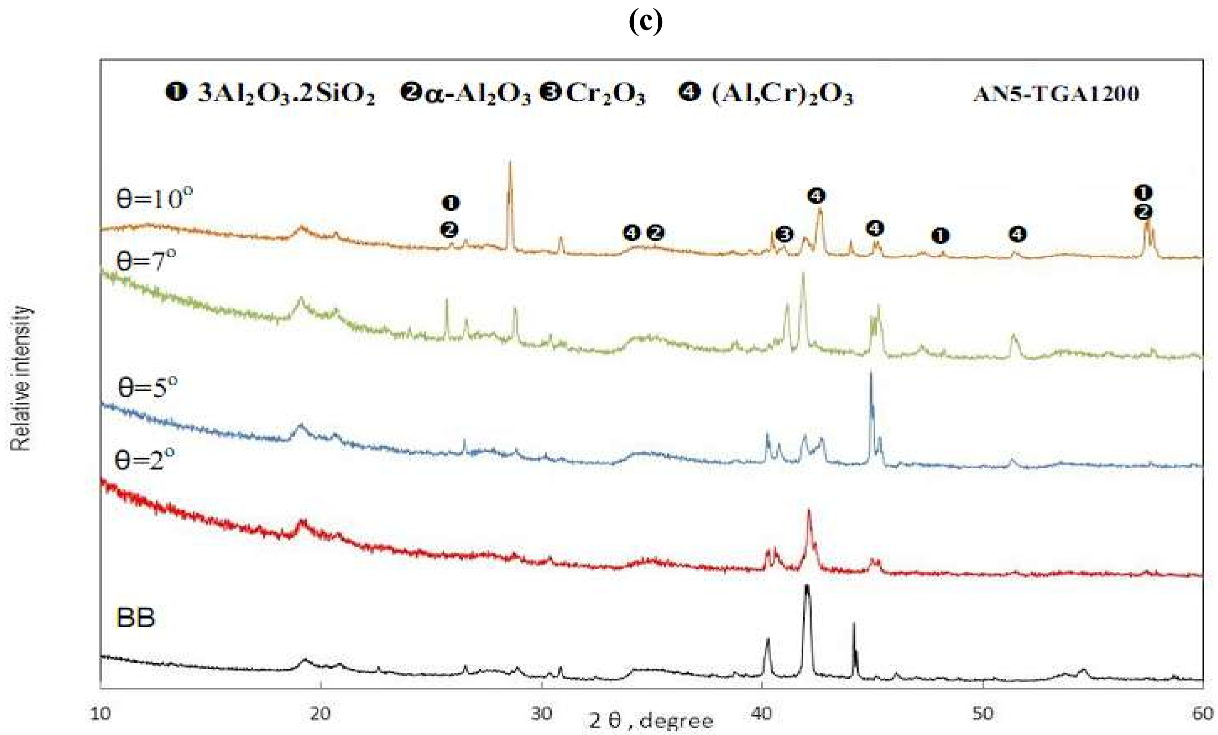

Figure 7.12 Glancing angle XRD data at different incident beam angles (θ) of the scale formed on the oxidized AN5 specimen at (a) 800 ^{o}C, (b) 1000 ^{o}C and (c) 1200 ^{o}C (BB refer to Bragg Brentano geometry diffraction pattern taken from TGA cube sample before isothermal oxidation experiment)

(a)

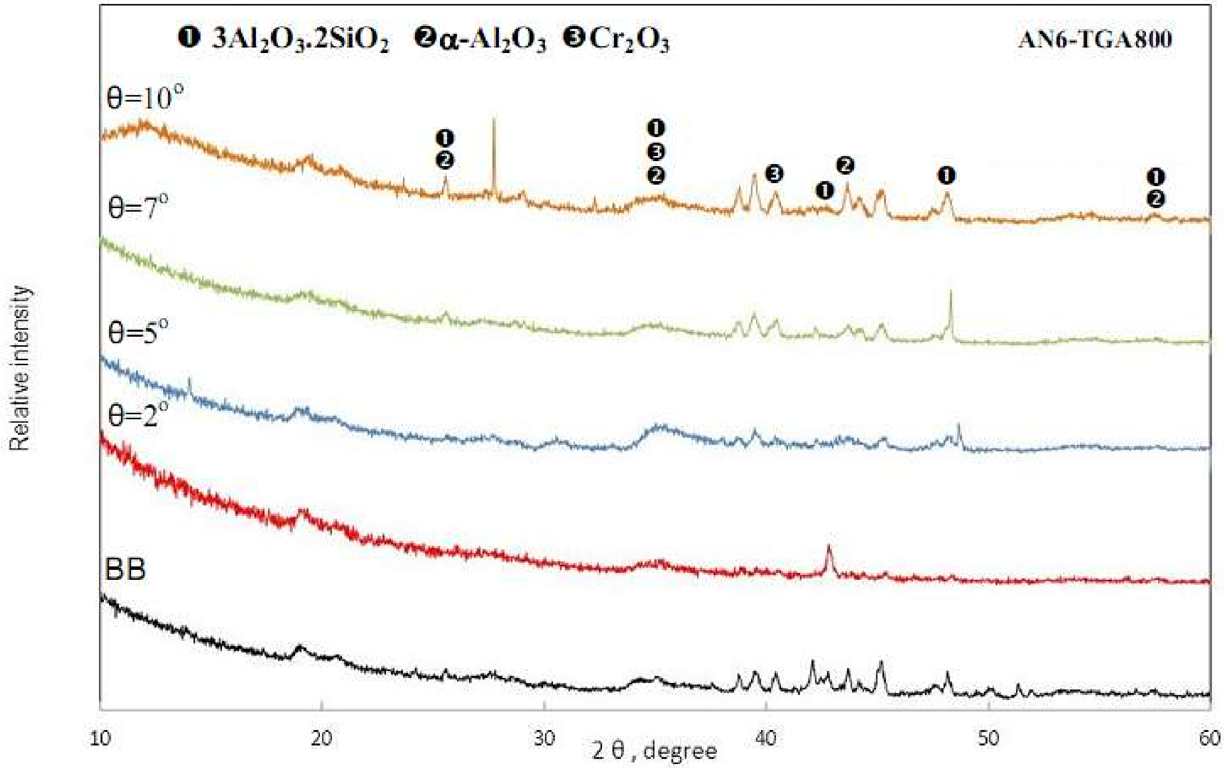
❶ $3Al_2O_3.2SiO_2$ ❷ α-Al_2O_3 ❸ Cr_2O_3
AN6-TGA800
θ=10°
θ=7°
θ=5°
θ=2°
BB
❶❷
❶❸❷
❸
❶
❷
❶
❶❷
Relative intensity
10
20
30
40
50
60
2 θ , degree

(b)

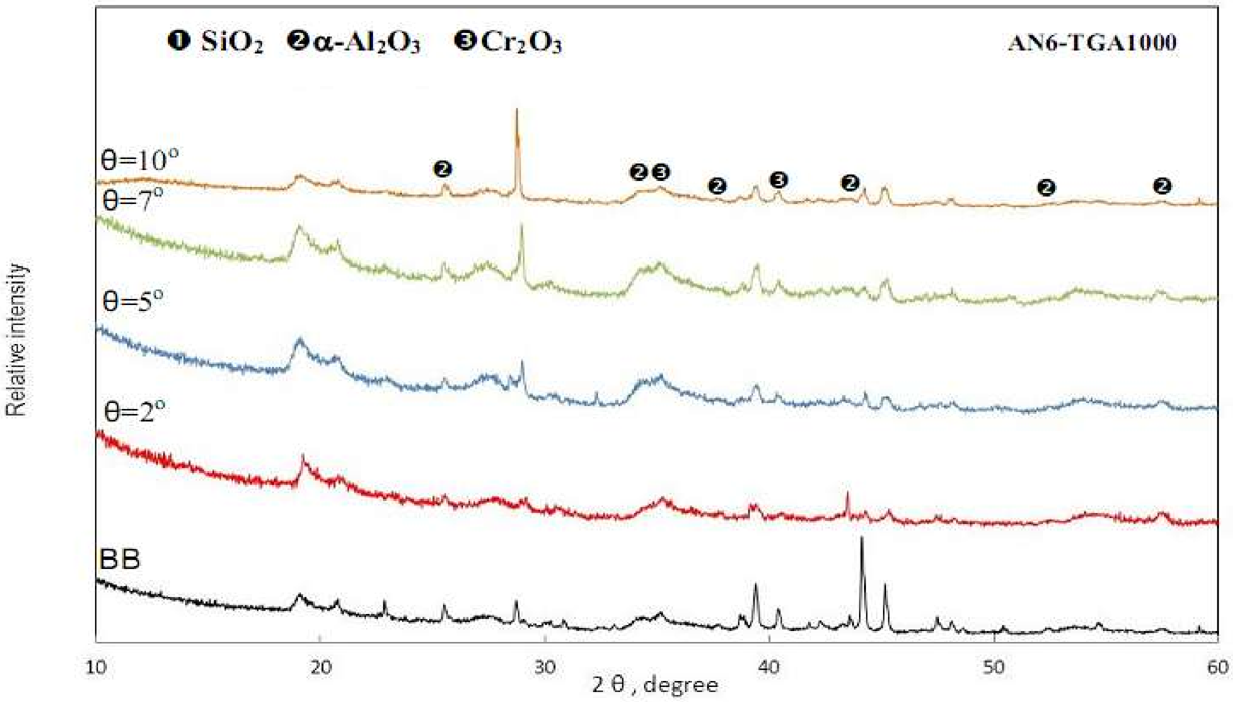
❶ SiO_2 ❷ α-Al_2O_3 ❸ Cr_2O_3
AN6-TGA1000
θ=10°
θ=7°
θ=5°
θ=2°
BB
❷
❷❸
❷
❸
❷
❷
❷
Relative intensity
10
20
30
40
50
60
2 θ , degree

(c)

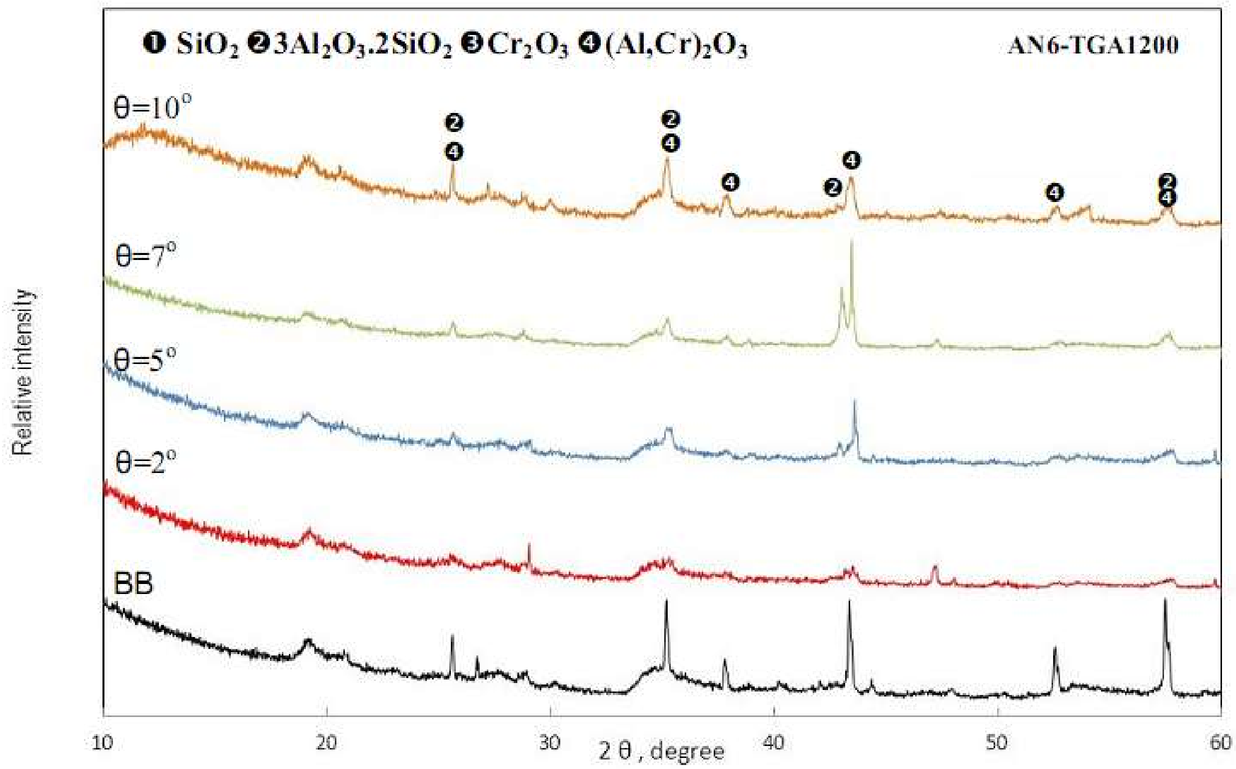

Figure 7.13 Glancing angle XRD data at different incident beam angles (θ) of the scale formed on the oxidized AN6 specimen at (a) 800 °C, (b) 1000 °C and (c) 1200 °C (BB refer to Bragg Brentano geometry diffraction pattern taken from TGA cube sample before isothermal oxidation experiment)

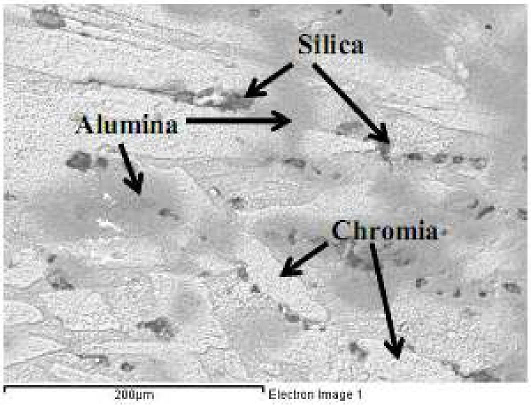

Figure 7.13.1 Surface SEM-BSE image of oxidized specimen of AN5 at 1000 °C

7.3. Discussion

7.3.1 Microstructures of Cr-45Si-5Al-5Nb (alloy AN5)

The solidification microstructure of AN5-AC would suggest that the $(Nb,Cr)_6Si_5$ silicide was the primary phase. Considering the melting temperatures of Cr_5Si_3 and $CrSi_2$, of which that of the former is higher (see Figure 2.1), the solidification path of AN5 was $L \rightarrow L + (Nb,Cr)_6Si_5 \rightarrow L + (Nb,Cr)_6Si_5 + (Cr,Nb)_5(Si,Al)_3 \rightarrow (Nb,Cr)_6Si_5 + (Cr,Nb)_5(Si,Al)_3 + Cr(Si,Al)_2$. Consider the EDX data in Table 7-2, as the 6-5 silicide formed the surrounding melt became slightly richer in Cr, lean in Nb and rich in Al, in this melt the 5-3 silicide formed making the remaining liquid rich in Al and Si and lean in Cr and then the disilicide formed.

The aforementioned solidification path for AN5-AC can be compared with the calculated paths using the Pandat and ThermoCalc SSOL4 databases. For the nominal composition the former gives (with comments by the author in parenthesis) the following solidification path (see also Figure 7.14 a) :

2121 K LIQUID -> CrNbSi_T1 (where in Pandat CrNbSi_T1 = $(Cr,Nb)_6Si_5$)

1796 K LIQUID + CrNbSi_T1 -> Mo_5Si_3 (meaning tetragonal 5-3 silicide with prototype W_5Si_3, i.e., isomorphous with Cr_5Si_3, see section 2.2)

1796 K LIQUID -> Mo_5Si_3

1633 K LIQUID + Mo_5Si_3 -> CrSi

1591 K LIQUID -> CrSi + $CrSi_2$

1575 K LIQUID -> CrSi + $CrSi_2$ + CrNbSi_T1

873 K LIQUID + $CrSi_2$ + CrNbSi_T1 -> CrSi + FCC_A1

870 K LIQUID + CrSi + CrNbSi_T1 -> FCC_A1 + Mo_5Si_3

668 K LIQUID + CrNbSi_T1 + FCC_A1 + Mo_5Si_3

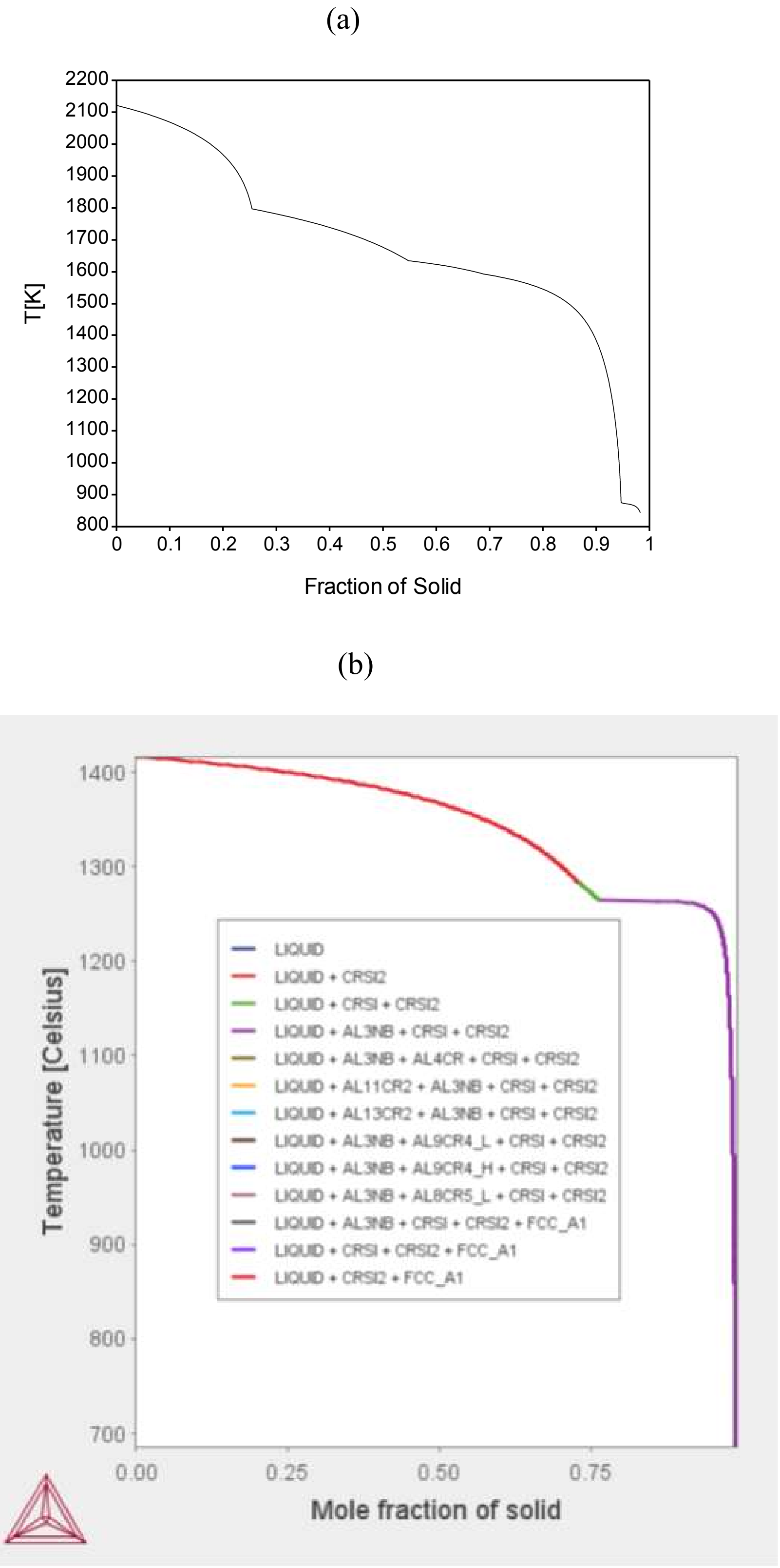

Figure 7.14 Solidification path for the alloy AN5-AC using a) Pandat database b) ThermoCalc SSOL4 database

According to Pandat the primary phase in AN5-AC should be the CrNbSi_T1 or $(Cr,Nb)_6Si_5$ silicide and this together with the tetragonal 5-3 silicide and Al should be the phases in the as solidified microstructure. The calculated path suggests a peritectic reaction between the 5-3 silicide and CrSi and a eutectic between CrSi and $CrSi_2$ (in agreement with the Cr-Si binary) and a ternary eutectic between CrSi, $CrSi_2$ and $(Cr,Nb)_6Si_5$ and that at the later stages of solidification the fcc Al forms. Compared with the cast microstructure of AN5-AC, Pandat accounts for the formation of the three observed phases.

The solidification path for the alloy AN5 using ThermoCalc SSOL4 database is shown in Figure 7.14 b. It is clear that ThermoCalc cannot account for the formation of primary $(Cr,Nb)_6Si_5$ silicide, and predicts formation of CrSi, $CrSi_2$ with Al_3Nb and Al-Cr aluminides such as Al_4Cr, $Al_{11}Cr_2$, $Al13_3Cr_2$, Al_9Cr_4, Al_8Cr_5 and fcc Al. Thus, the calculated path using ThermoCalc accounts only the formation of $CrSi_2$ but not of the 6-5 and 5-3 silicides.

The same phases that were observed in the cast microstructure were also present in the alloy AN5 after the two heat treatments, namely the $(Nb,Cr)_6Si_5$, $(Cr,Nb)_5(Si,Al)_3$ and $Cr(Si,Al)_2$, with no significant changes in the vol% of phases between HT1200 and HT1300. The solubility of Nb in the 6-5 silicide decreased slightly after the heat treatment at 1300 C while the compositions of $(Cr,Nb)_5(Si,Al)_3$ and $Cr(Si,Al)_2$ were essentially unchanged compared with the cast alloy, and the Si + Al content of the latter two silicides was as expected from the Cr-Si binary.

If Al and Si are taken as equivalent so that the alloy AN5 can be considered as Cr-50Si-5Nb, then the latter alloy falls in the three phase ($(Nb,Cr)_6Si_5$, $CrSi_2$ and CrSi) field of the 1200 ^{o}C isothermal section of the Nb-Cr-Si ternary by David et al. [150] that is included in the database of the ASM Alloy Phase Diagrams Centre (see Figure 7.15). If, however, the alloy is considered as Cr-45Si-10(Nb,Al) (the maximum solid solubility of Al in Nb is above 5 at%) then in the same isothermal the alloy is in the two phase Cr_5Si_3 and $Nb_2Cr_4Si_5$ field, see below. The above data for the cast and heat treated alloy AN5 would thus suggest that the synergy of Al, Si and Nb in AN5 suppressed the formation of CrSi and stabilised an M_6Si_5 type silicide and the $CrSi_2$, as was the case with the synergy of Al, Si and Hf in the alloy AN1. It is thus suggested that the equilibrium microstructure of AN5 at 1200 °C and 1300 °C consists of the $(Nb,Cr)_6Si_5$, $(Cr,Nb)_5(Si,Al)_3$ and $Cr(Si,Al)_2$ phases with the volume fractions and chemical compositions that are given in Tables 7.1 and 7.2.

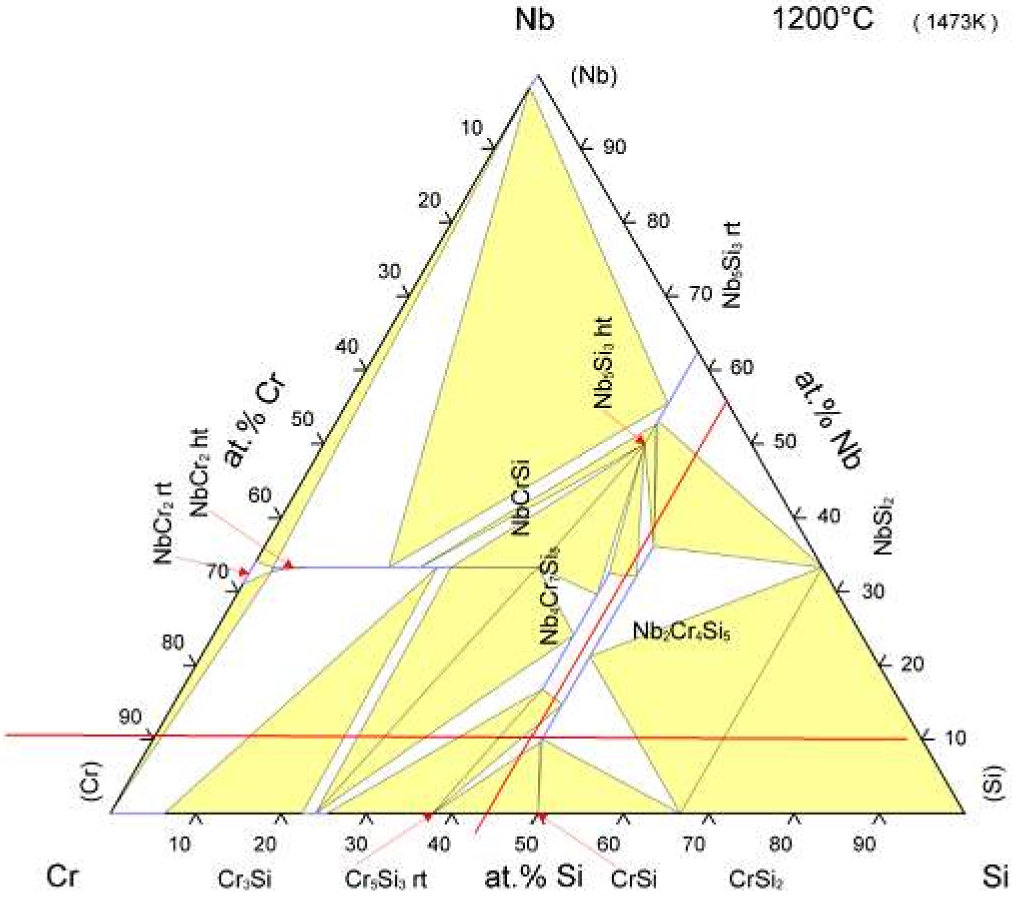

© ASM International 2010. Diagram No. 204961

Figure 7.15 The isothermal section of Cr-Nb-Si ternary system at 1200 °C [150]

7.3.2 Microstructures of Cr-25Si-25Al-5Nb (alloy AN6)

The solidification microstructure of AN6-AC contained the 11-8 ($Cr_{11}Ge_8$-type) orthorhombic $(Nb,Cr)_{11}(Si,Al)_8$ silicide in addition to the 6-5 (V_6Si_5-type) orthorhombic $(Nb,Cr)_6(Si,Al)_5$ and 5-3 silicides, see Table 7.3. We have seen in the previous section that the melting temperature of the 6-5 silicide is higher than that of the 5-3 (the former was the primary phase in AN5) but from the microstructure of AN6-AC shown in Figure 7.4 a, b it is not easy to deduce if the 11-8 or the 6-5 silicide was the primary phase in this alloy. The 11-8 and 6-5 silicides exist in the Nb-Cr-Si system; see Table 2-4 in section 2.14 which suggests that the equilibria between Nb, Cr and Si determined the early stages of solidification. For the latter ternary system Cornish et al. [151] give at $T \leq 2200\ ^{o}C$ the U1 reaction $L + (Nb,Cr)_6Si_5 \rightarrow (Nb,Cr)_{11}(Si,Al)_8 + \beta Nb_5Si_3$ which means that the 6-5 silicide forms before the 11-8 one. If in the alloy AN6 the Al and Si are considered as equivalent so that the alloy can be considered as Cr-50Si-5Nb, then in the liquidus projection given by Cornish et al. [151] and Shao [51] the alloy falls in the $(Nb,Cr)_6Si_5$ phase region, in other words the 6-5 silicide is the primary phase and is followed the 11-8 and 5-3 silicides.

According to Zhao et al. [52] the former two silicides (i.e., the 11-8 and 6-5 silicides) are essentially line compounds with different Cr/Nb ratio and stoichiometric concentration of Si. As the aforementioned reaction occurred the remaining liquid became leaner in Nb and Si and Cr and very rich in Al (see Table 7-3), the equilibria between Cr, Al and Si determined the later stages of solidification and Cr aluminides formed, first the Cr_5Al_8 and then the Cr_4Al_9 as the former has a higher melting point than the latter according to the Al-Cr binary phase diagram. The formation of the latter aluminides is possible via the reactions U5 (at 1188 ^{o}C) $L + Cr_5Si_3 \rightarrow CrSi_2 + \gamma\text{-H}\ ((Cr_5(Si,Al)_8)$ and P1 (at 1174) $L + CrSi_2 + \gamma\text{-H} \rightarrow \tau_4\ ((Cr_4(Si,Al)_9)$ and would thus suggest that the synergy of Cr, Al, Si with Nb in AN6 (i.e., at a lower Al/Si ratio compared with AN5) suppressed the $CrSi_2$ compound (the latter was stable in AN5, see above). Thus, it is suggested that the solidification path of AN6 was $L + (Nb,Cr)_6Si_5 \rightarrow (Nb,Cr)_{11}(Si,Al)_8 + \beta Nb_5Si_3$ (i.e., tetragonal 5-3 silicide) $\rightarrow L + (Nb,Cr)_{11}(Si,Al)_8 + \beta Nb_5Si_3 + Cr_5(Si,Al)_8 \rightarrow (Nb,Cr)_{11}(Si,Al)_8 + \beta Nb_5Si_3 + Cr_5(Si,Al)_8 + Cr_4(Si,Al)_9$.

The aforementioned solidification path for AN6-AC can be compared with the calculated paths using the Pandat and ThermoCalc SSOL4 databases. For the nominal composition of AN6 the former gives (with comments by the author in parenthesis) the following solidification path (see also Figure 7.16 a) :

2068 K LIQUID -> CrNbSi_T1 (where in Pandat CrNbSi_T1 = $(Cr,Nb)_6Si_5$)

1715 K LIQUID -> CrNbSi_T1 + A15_Nb_3Al (the Cr_3Si is also an A15 compound)

1647 K LIQUID + CrNbSi_T1 -> A15_Nb_3Al + Mo_5Si_3 (meaning tetragonal 5-3 silicide with prototype W_5Si_3, i.e., isomorphous with Cr_5Si_3, see section 2.2)

1647 K LIQUID -> A15_Nb_3Al + Mo_5Si_3

1402 K LIQUID+A15_Nb_3Al+Mo_5Si_3

(a)

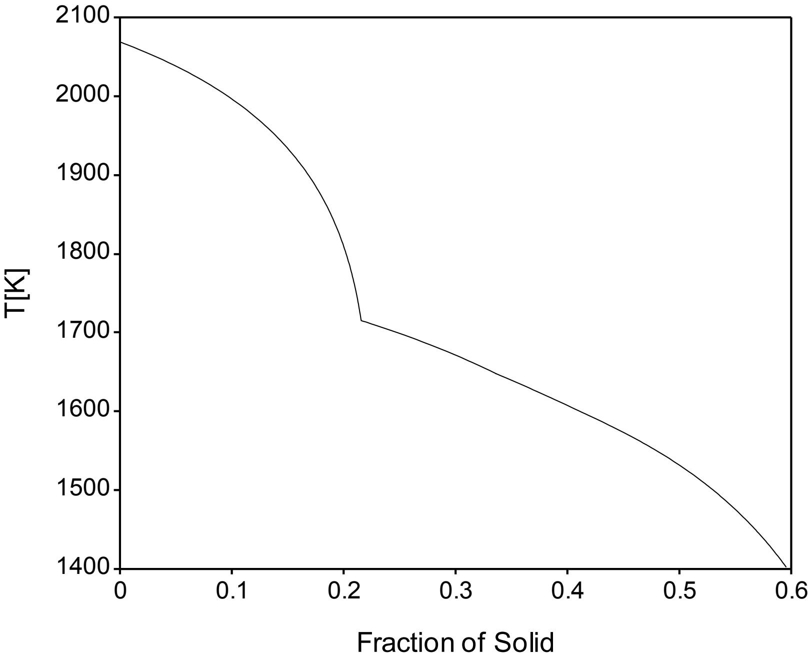

(b)

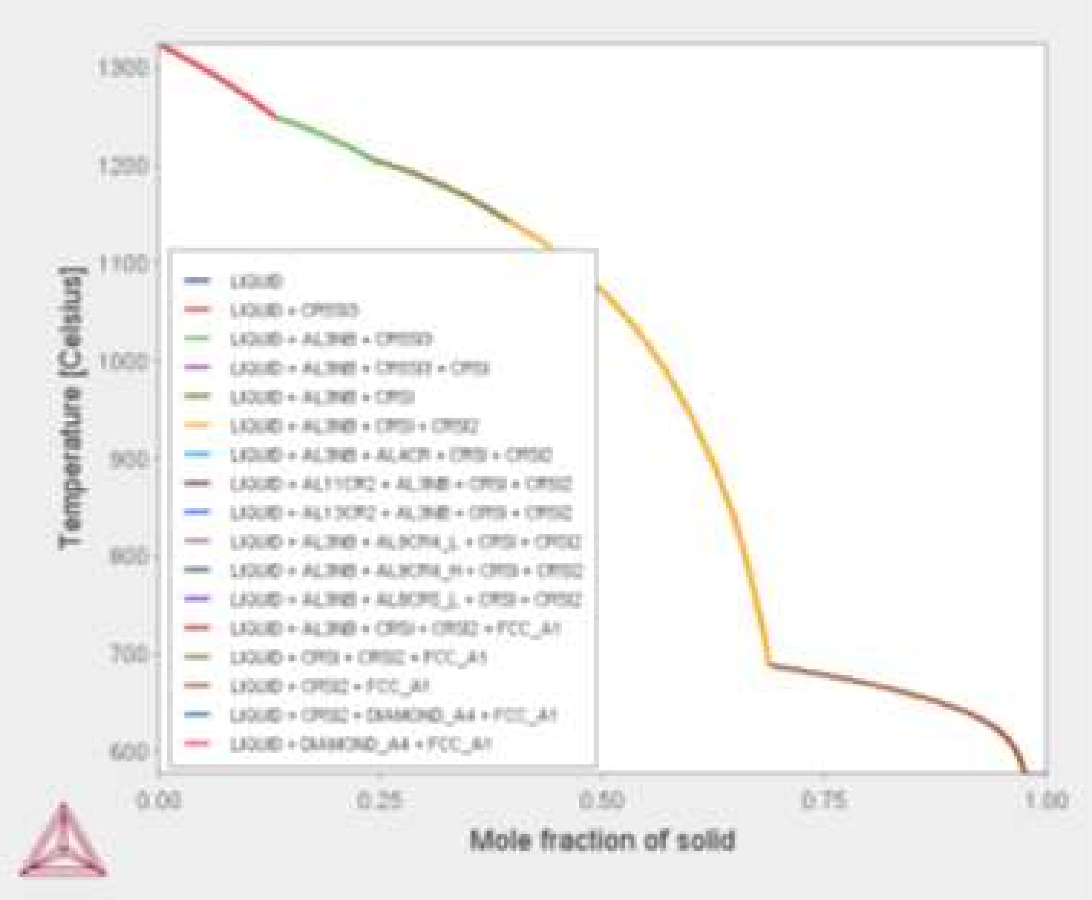

Figure 7.16 Solidification path for the alloy AN6-AC using a) Pandat database b) ThermoCalc SSOL4 database

The solidification path for the alloy AN6-AC using ThermoCalc SSOL4 database is shown in Figure 7.16 b. Despite the prediction of 6-5 silicide by Pandat and ThermoCalc, both databases cannot account for the 11-8 silicide, Pandat predicts formation of A15 intermetallic which was not observed in AN6-AC, accounts for the tetragonal 5-3 silicide but not the two Cr aluminides. ThermoCalc can account for the 6-5 silicide, correctly predicts formation of the 5-3 silicide and the two Cr aluminides, observed in AN6-AC but in addition predicts formation of many other intermetallics and Al none of which was observed.

Even though Si and Al macro-segregation was not suggested by the EDX data for AN6-AC (see Table 7.3), it was decided to use both databases to calculate the solidification paths for two alternative Si richer compositions, close to the nominal composition of AN6, namely Cr-26Si-

24.5Al-5Nb (at%)and Cr-27Si-23.5Al-5Nb (at%). The Pandat predicted respectively the solidification paths

2074 K LIQUID -> CrNbSi _T1
1705 K LIQUID -> CrNbSi _T1 + A15_Nb_3Al
1686 K LIQUID + CrNbSi _T1 -> A15_Nb_3Al + Mo_5Si_3
1686 K LIQUID -> A15_Nb_3Al + Mo_5Si_3
1422 K LIQUID+A15_Nb_3Al+Mo_5Si_3

and

2082 K LIQUID -> CrNbSi_T1
1709 K LIQUID + CrNbSi_T1 -> Mo_5Si_3
1709 K LIQUID -> Mo_5Si_3
1671 K LIQUID -> A15_Nb_3Al + Mo_5Si_3
1448 K LIQUID+A15_Nb_3Al+ Mo_5Si_3

In other words the same primary phase and the same phases in the last to solidify melt as for the nominal composition, with a delay in the formation of the A15 intermetallic as the Si/Al ratio in the alloy increased.

ThermoCalc also predicted the same primary phase and the same phases in the last to solidify melt as for the nominal composition (see above), with a delay in the formation of the A15 intermetallic as the Si/Al ratio in the alloy increased.

After the heat treatment at 1200 ^{o}C there was liquation in the material owing to melting of the Cr_4Al_9 which was present at a small vol.% in the cast microstructure (see Table 7-1). This led to significant coarsening of the microstructure in which the 11-8 and 6-5 silicides were no longer present and the vol.% of the 5-3 silicide increased by ~ 63% compared with the cast alloy (Table 7-1). The microstructure of AN6-HT1200 consisted of the 5-3 silicide and the 5-8 Cr aluminide (Table 7-3), while that of AN6-HT1300 consisted of the same phases plus the τ_4 (($Cr_4(Si,Al)_9$). If we were to consider the AN6-HT1200 and AN6-HT1300 as ternary Cr-Si-Al alloys with actual Al and Si contents as given in Table 7-3 and the 1100 ^{o}C isothermal section proposed by Liang et al. [40] (Figure 7.17) then the heat treated alloys are very close to the 5-3 plus γ-H or 5-3 plus γ-H plus τ_4 two or three phase fields, which would suggest that the heat treated microstructures were "controlled" by the Cr-Si-Al phase equilibria.

The data for the alloy AN6 would thus suggest that if Cr-25Si-25Al were to be used as bond coat (BC) alloy on a Nb silicide based alloy, diffusion of Nb from the substrate to the BC could lead to control of the phase equilibria of Cr, Al and Si at high temperatures, and thus liquation at T > 1100 ^{o}C owing to formation of Cr aluminides.

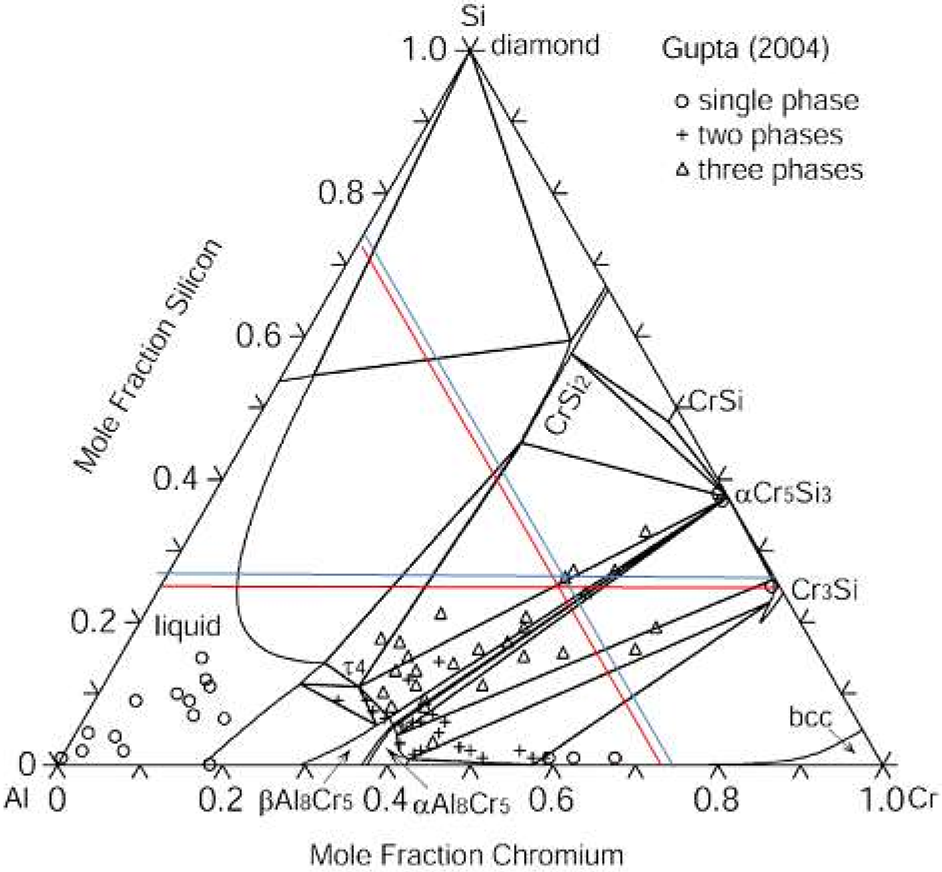

Figure 7.17 The 1100 ^{o}C isothermal section of Al-Cr-Si proposed by Liang et al [40].

7.3.3 Oxidation of the alloys AN5 and AN6

Table 7-6 summarises the scales formed on the two alloys at 800, 1000 and 1200 °C. The oxidation of the alloys AN5 and AN6 at 800 °C lead to interesting observations concerning the behaviour of silicides and aluminides precursor phases. Both alloys did not show any sign of accelerated or pest oxidation. According to the Cr-Si-O ternary system by Matskevich et al., the silica is in equilibrium with $CrSi_2$, CrSi, Cr_5Si_3 and Cr_3Si silicides and thus silica could be expected to form on the surface of the alloy up to 1000 °C, in other word, the Cr silicides can form silica up to this temperature. In contast, according to Grabke et al. [88] the $CrSi_2$ forms chromia in the temperature range 900 to 1050 °C in spite of the fact that the Cr activity in the $CrSi_2$ is lower than the Si activity the concentration of which is high in the disilicide.

Table 7-6 Summary of oxide scales formed on the alloy AN5 and AN6.

Alloy	Temperatures		
	800 °C	1000 °C	1200 °C
Cr-45Si-5Al-5Nb (AN5)	Whiskers SiO_2-Al_2O_3-Cr_2O_3-Nb_2O_5 Mullite No spallation	Cells/whiskers SiO_2-Al_2O_3-Cr_2O_3-Mullite No spallation	Continuous scale Al_2O_3-Cr_2O_3 $(Al,Cr)_2O_3$ Mullite Partial spallation
Cr-25Si-25Al-5Nb (AN6)	Whiskers SiO_2-Al_2O_3-Mullite-Nb_2O_5 No spallation	Cell Al_2O_3-Cr_2O_3 –Nb_2O_5 Continuous scale No spallation	Buckeled scale $(Al,Cr)_2O_3$ Mullite Partially Spalled in ridges

The alloy AN5 consisted of the Nb_6Si_5, Cr_5Si_3 and $Cr(Si,Al)_2$ intermetallics. According to the data obtained from EDX analysis of the scale (Table 7-7), the glancing angle XRD (Figure 7.12 a) and EDX study of the scale, see Figure 7.18 mixtures of silica , alumina, mullite and chromia were fomred on the surface. In the alloy AN6, which consited of the Nb_6Si_5, $Nb_{11}Si_8$, Cr_5Si_3, Cr_5Al_8 and Cr_4Al_9 precursor phases in its as-cast microstructure, the scale contained mullite, alumina and chromia, see Figure 7.13 a, 7.19 and Table 7-8. The oxide formed on the

AN6 alloy was rather continuous and smooth compared with alloy AN5 on which the scale had rough morphology. This could be related to the different growth rates of oxides species on

Table 7-7 Quantitative EDX analysis (at.%) of the scale formed on the alloy AN5 at 800 ^{o}C, The spectra are from Figure 7.18 a.

Spectrum	O	Al	Si	Cr	Nb
Spectrum 1	50.25	34.77	4.46	10.53	
Spectrum 2	38.23	9.89	16.56	34.79	0.53
Spectrum 3	51.15	32.52	5.01	10.85	0.47
Spectrum 4	46.11	26.94	7.44	19.51	
Spectrum 5	49.53	28.05	6.38	16.05	
Spectrum 6	53.07	19.03	11.24	13.95	2.71
Spectrum 7	46.97	18.75	11.16	21.99	1.12
Spectrum 8	45.77	19.87	13.14	18.94	2.28

Table 7-8 Quantitative EDX analysis (at.%) of the scale formed on the alloy AN6 at 800 ^{o}C. The spectra are from Figure 7.19 a

Spectrum	O	Al	Si	Cr	Nb
Spectrum 1	43.18	16.21	-	40.61	-
Spectrum 2	52.89	37.80	1.10	8.21	-
Spectrum 4	50.12	38.61	0.91	10.36	-
Spectrum 6	52.35	37.41	1.05	8.94	0.25
Spectrum 7	56.75	36.27	1.26	5.72	-
Spectrum 8	62.31	29.10	4.77	3.83	-
Spectrum 9	52.25	38.59	0.86	8.11	0.19
Spectrum 10	59.52	34.35	1.36	4.44	0.34
Spectrum 11	52.49	37.39	1.06	8.78	0.29

(a)

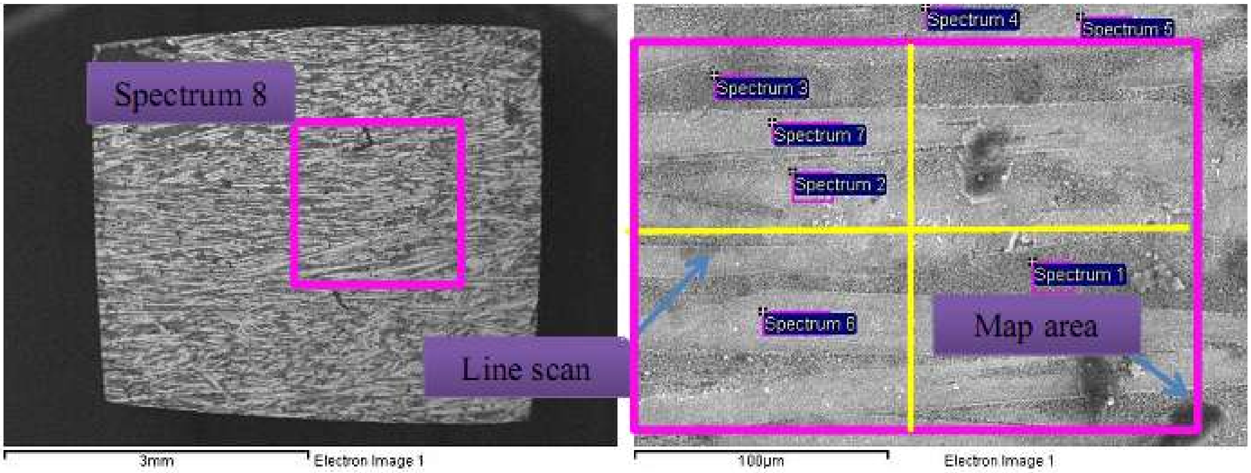
Spectrum 8
Spectrum 4
Spectrum 5
Spectrum 3
Spectrum 7
Spectrum 2
Spectrum 1
Spectrum 6
Map area
Line scan
3mm
Electron Image 1
100µm
Electron Image 1

(b)

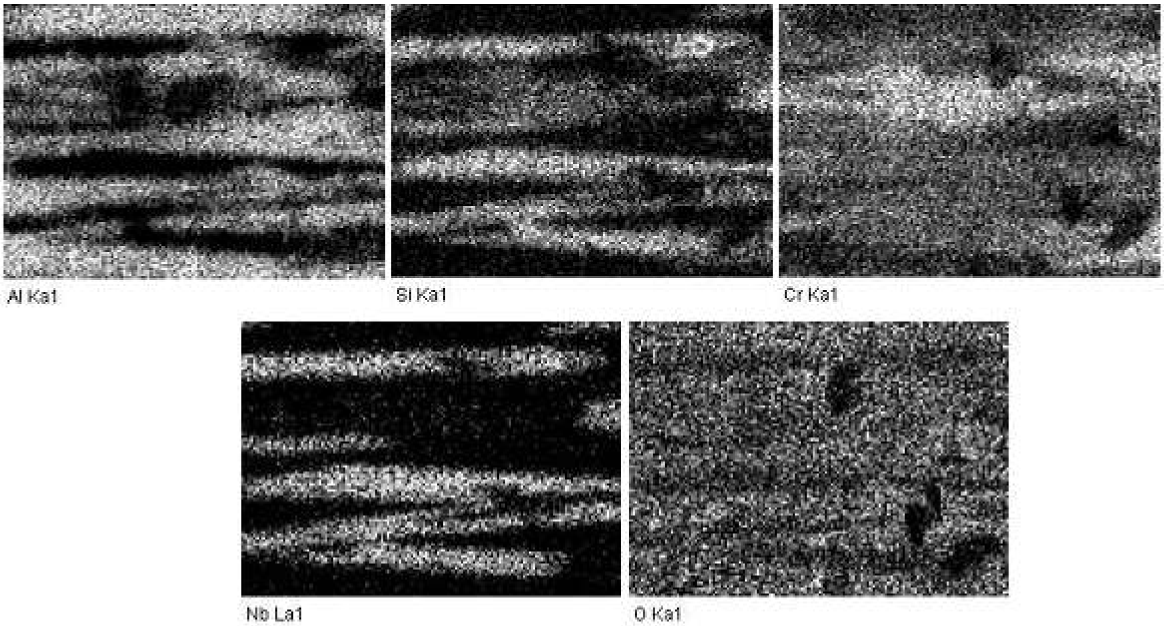
Al Ka1
Si Ka1
Cr Ka1
Nb La1
O Ka1

(c1): horizontal line scans

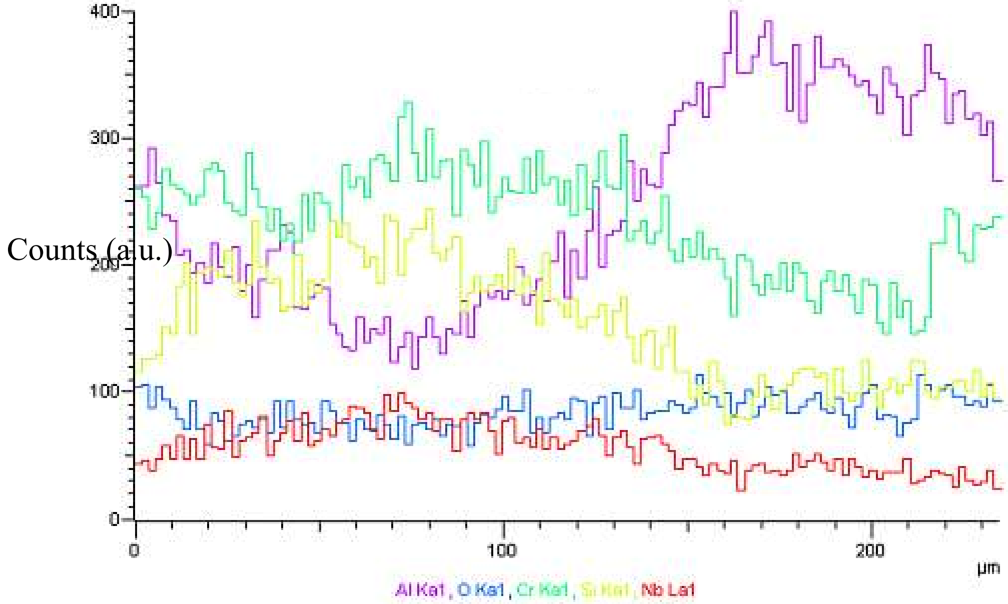

(c2): vertical line scans

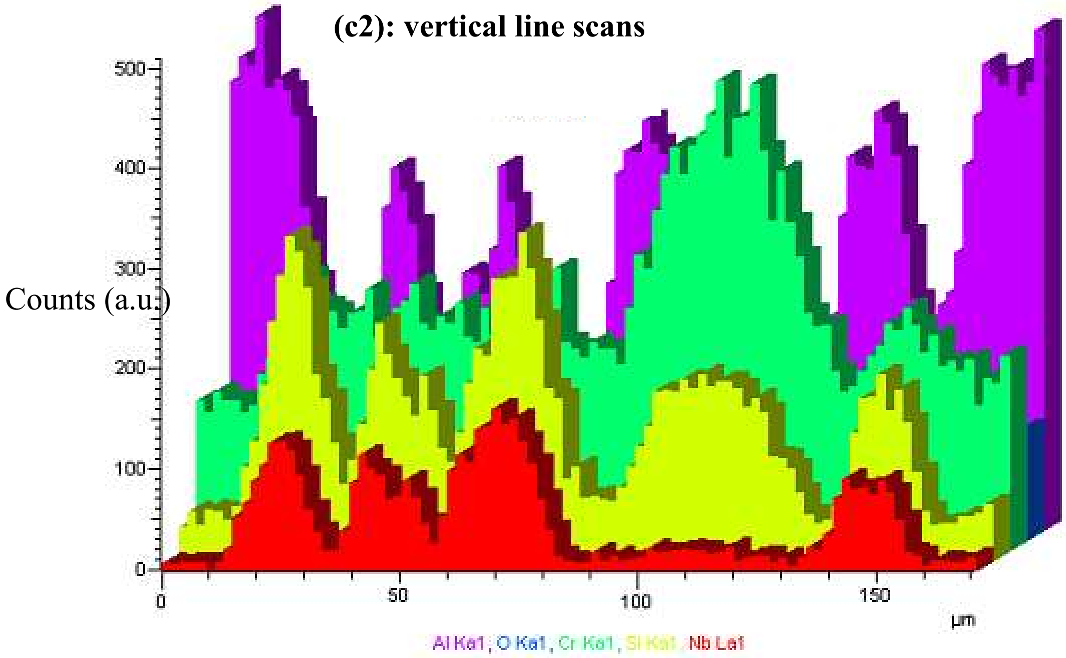

Figure 7.18 a) Surface SEM-BSE image of oxidized specimen of AN5 at 800 °C b) surface elemental maps of Al, Si, Cr, Nb and O of the oxidized specimen and c) line scans of the oxidized specimen

(a)

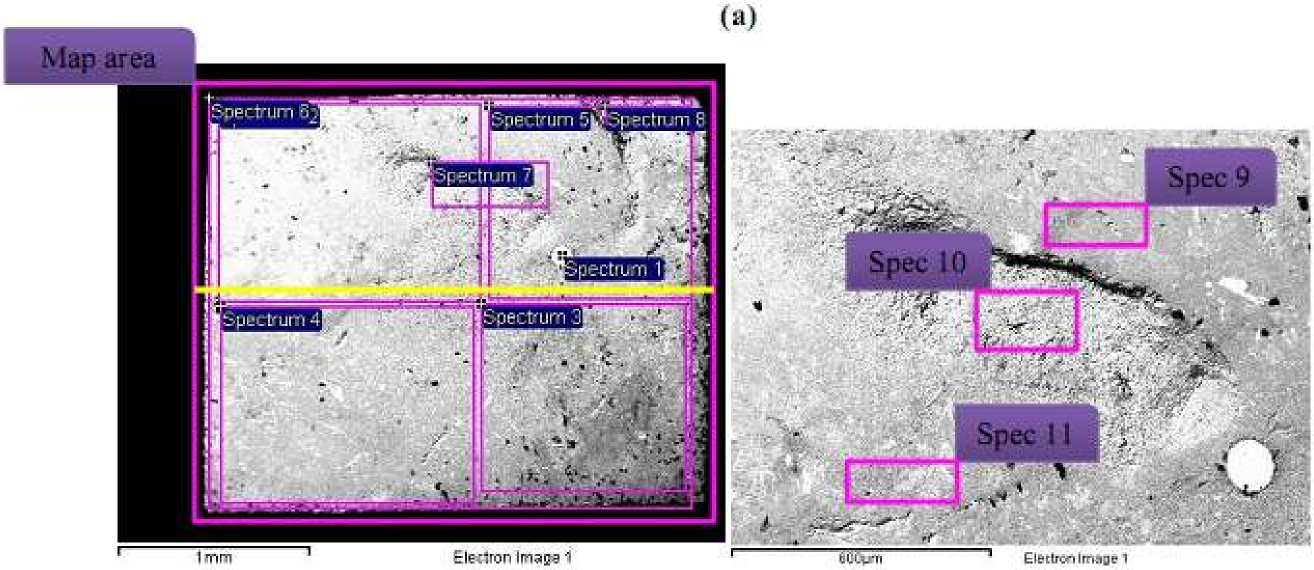
Map area
Spectrum 6
Spectrum 5
Spectrum 8
Spectrum 7
Spectrum 1
Spectrum 4
Spectrum 3
1mm
Electron Image 1
Spec 9
Spec 10
Spec 11
600µm
Electron Image 1

(b)

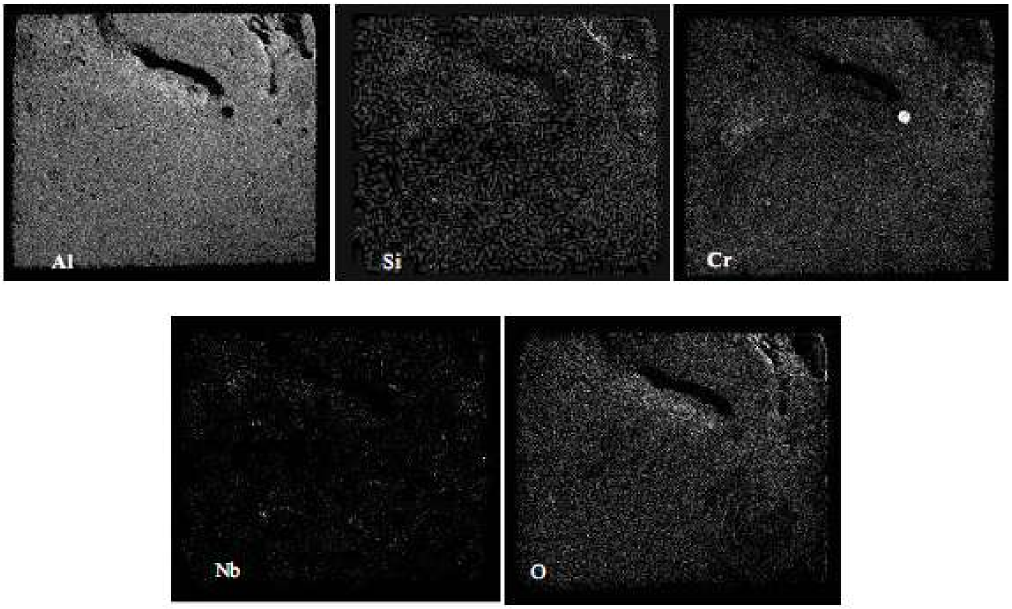
Al
Si
Cr
Nb
O

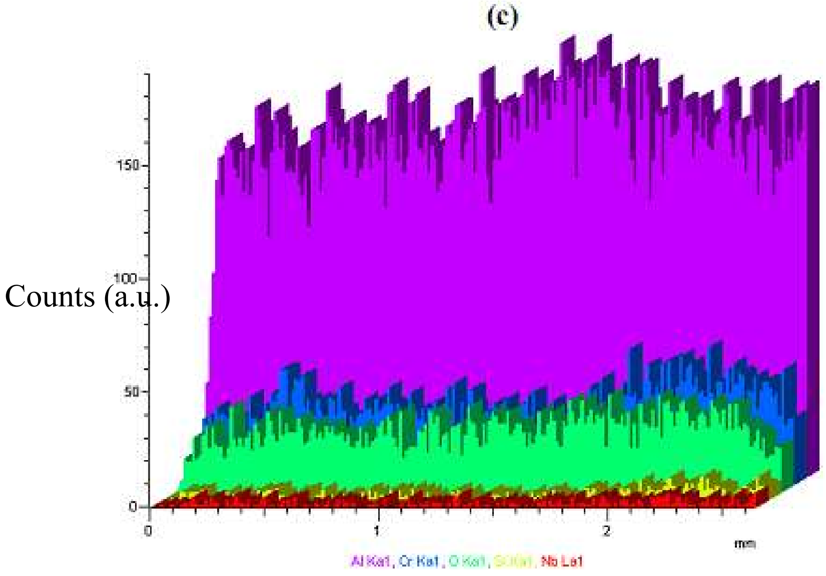

Figure 7.19 (a) Surface SEM-BSE image of oxidized specimen of AN6 at 800 ^{o}C, (b) surface elemental maps of Al, Si, Cr, Nb and O and (c) line scans of the oxidized specimen(yellow line)

different precursors in the alloy where the growth rate of the oxide depends upon the upward diffusion of Si and/or Al and inward diffusion of the oxygen. The oxidation rate constant of the AN5 alloy at 800 ^{o}C indicated that the alloy oxidized with a higher than parabolic rate for the first 17 hours exposure and the oxidation was controlled by diffusion of Si, Cr and/or Al from the substrate. In contrast in the alloy AN6, parabolic oxidation behaviour was found during the whole isothermal oxidation where the oxidation of the alloy was controlled by diffusion of the Al and Cr from the substrate to the surface. It is concluded that in the alloy AN5, the high Al solubility in $CrSi_2$ decreased the activity of Si and promotes the formation of chromia instead of silica. Therefore, the Al addition suppressed the selective oxidation of Si in the $CrSi_2$. Silica formed on the surfaces of Cr_5Si_3 and $(Nb,Cr)_6Si_5$ (Figure 7.20) by selective oxidation of Si [125]. The Al reservoir in the alloy AN6 was larger than AN5 as the microstructure of the former contained about 37 % aluminide that can form alumina. There was no evidence for formation of a solid solution between chromia and alumina (Corundum SS) in both the AN5 and AN6 alloys at 800 ^{o}C. This is in a good agreement with the Cr_2O_3-Al_2O_3 binary phase diagram [127]. The miscibility gap of Cr_2O_3 and Al_2O_3, shown in Figure 7.21 (a), indicates that alumina and chromia are immiscible at 800 °C in the composition range 0 to 0.85 mole fraction of chromia. The mullite solid solution phase was formed in both alloys at 800 °C whereby in the alloy AN5 the mullite and silica are stable in a two phase region and in the alloy AN6 the mullite and alumina are stable in a two phase region. According to the Cr_2O_3-Al_2O_3-SiO_2 ternary phase diagram in Figure 7.21 (b), the formation of the mullite, silica and corundum is feasible at lower temperature. The Nb as a reactive element added to the AN5 and AN6 alloys did not form a continuous niobium oxide (Figure 7.12 a and 7.13 a) but indeed patches of Nb_2O_5 (Figure 7.10 a5 and Figure 7.11 a5) were formed. The Ellingham diagram in Figure 7.22 shows that the reactive element oxide are more thermodynamically stable with oxygen than Cr/Cr_2O_3, typically exhibiting stabilities in the range of Si/SiO_2 to Al/Al_2O_3. The observation of patches of Nb_2O_5 in AN5 and AN6 can be related to the low activity of Nb in the precursor phases of the alloys.

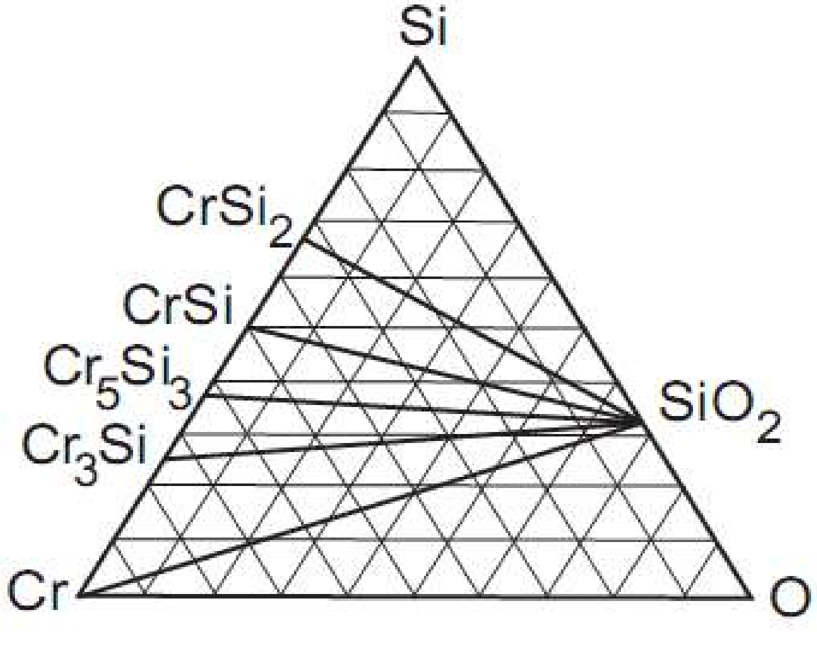

Figure 7.20 Ternary phase diagrams of Cr-Si-O system (T=373-1273 K) [125]

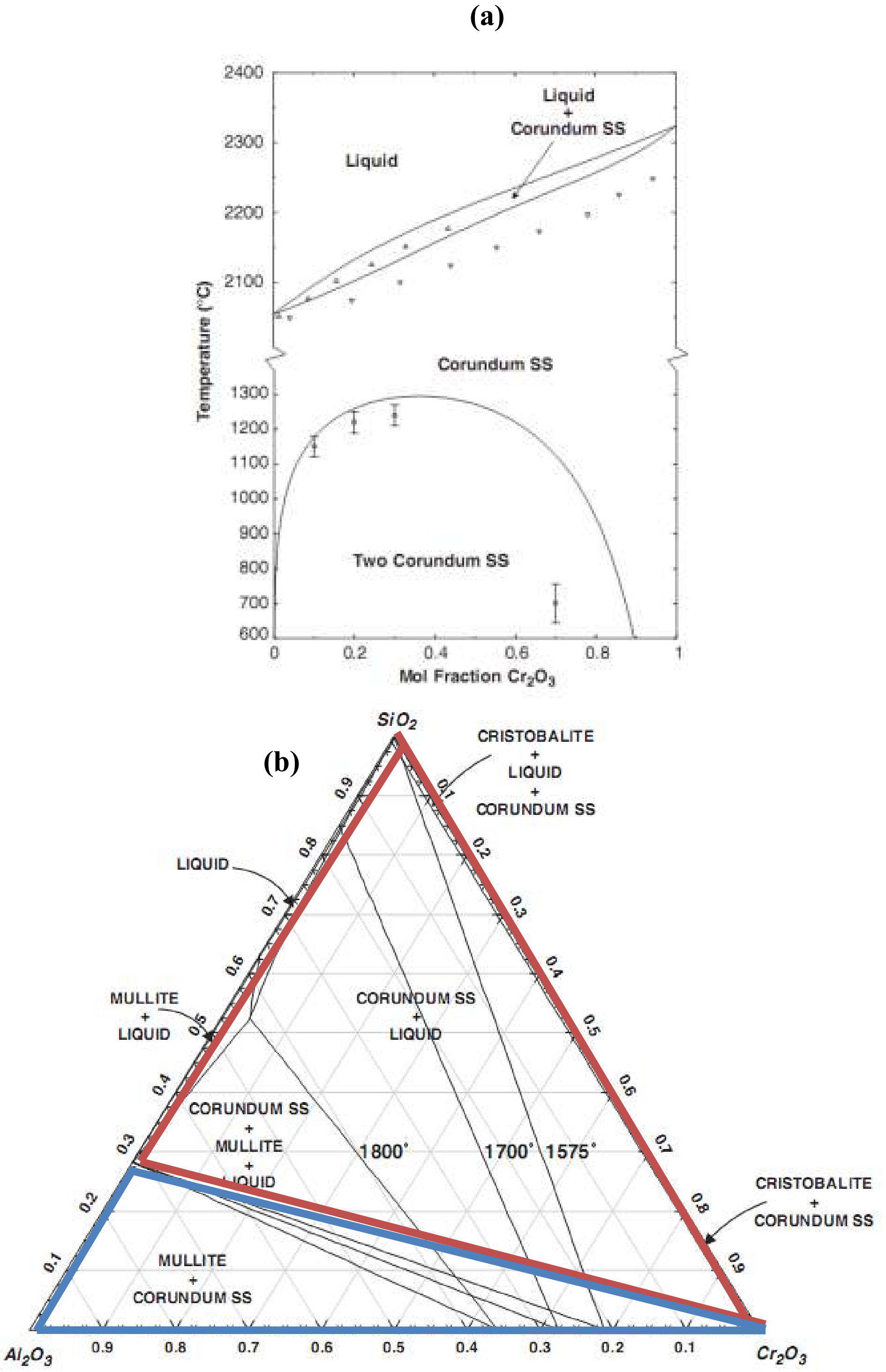

Figure 7.21 (a) Computed Al_2O_3-Cr_2O_3 phase diagram with the experimental solidus (▽) and liquidus (Δ) values of Bunting and the miscibility gap determination of Sitte (o), (b) Computed ternary phase diagram for Al_2O_3-Cr_2O_3-SiO_2 indicating isothermal section at 1575,1700,and1800 °C [127].

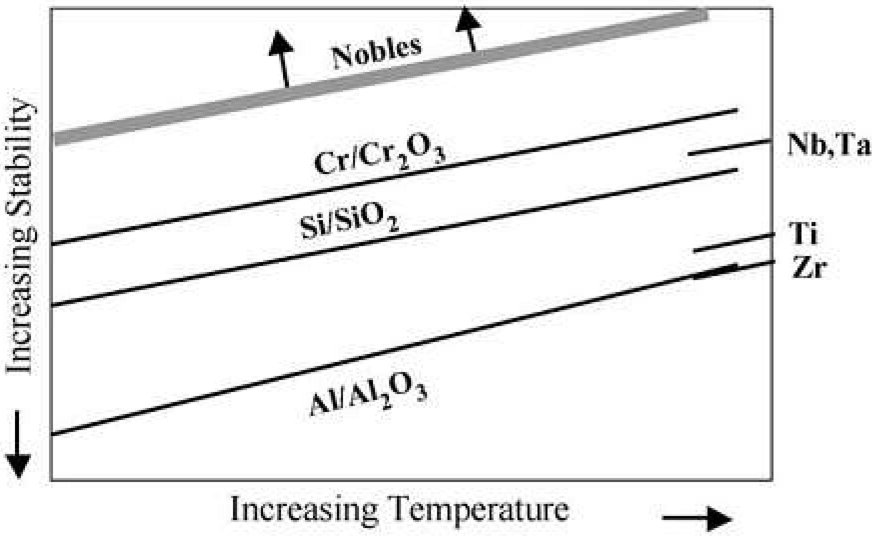

Figure 7.22 Ellingham diagram for oxides [6].

At 1000 and 1200 °C, the oxidation of the alloy AN5 changed to cube and parabolic oxidation behaviour, respectively. This behaviour was valid for limited exposure time during which the rate of protective scale formation was higher than the chromia volatilization in the alloy, which leads to a negative slope in the oxidation curves. The latter could also occur because of partial scale spallation and formation of a new subscale that eventually affected the ability of Al, Si, Cr fluxes to form a continuous protective scale. The formation of geometrical holes at the alloy/scale interface supports this argument. The serration shown in the oxidation curve of the alloy AN5 Figure 7.7 can also be due to scale spallation and formation of new scale on the substrate.

The scale formed on the alloy AN5 at 1000 °C consisted of a mixture of silica, alumina, chromia and mullite (Figure 7.12 b and 7.23). The mullite solid solution phase was dispersed in the scale as round shape particle, see also the EDX data in Table 7-9 and Figure 7.23 a, b and the glancing angle XRD in Figure 7.12 b. As mentioned earlier, there is a miscibility gap for chromia and alumina oxides where the oxides are stable together and this is related to the mole fraction of chromia and to temperature, Figure 7.21(a), Chromia and alumina cannot be present as solid solution unless the Cr concentration is either less than 1.6 at.% or more than 32 at.% at 1000 °C. The concentration of the Cr is 33.8 at.% (Table 7-9) which is outside of the

Table 7-9 Quantitative EDX analysis of the scale formed on the alloy AN5 at 1000 ^{o}C. The spectra are from Figure 7.23 a

Spectrum	**O**	**Al**	**Si**	**Cr**	**Nb**
Spectrum 1	58.02	15.68	3.34	22.56	0.40
Spectrum 2	57.01	30.71	1.18	10.84	0.25
Spectrum 3	58.82	0.89	0.72	39.18	0.38
Spectrum 4	62.89	2.40	0.57	33.80	0.34
Spectrum 5	57.52	29.76	1.27	11.21	0.25
Spectrum 6	61.65	10.29	26.53	1.53	-

Table 7-10 Quantitative EDX analysis of the scale formed on the alloy AN6 at 1000 ^{o}C. This spectra are from Figure 7.24 a

Spectrum	**O**	**Al**	**Si**	**Cr**	**Nb**
Spectrum 5	54.74	39.87	0.54	2.55	2.29
Spectrum 6	56.43	34.32	1.73	7.04	0.48
Spectrum 7	56.62	34.35	1.70	6.76	0.58
Spectrum 8	56.98	33.80	1.73	6.88	0.62
Spectrum 9	57.19	33.94	1.78	6.38	0.72
Spectrum 10	58.31	34.11	1.33	5.15	1.11
Spectrum 11	45.49	50.49	2.84	1.18	-
Spectrum 12	46.87	49.27	2.17	-	1.69
Spectrum 13	47.94	45.27	2.46	4.33	-
Spectrum 14	49.49	42.18	3.10	5.22	-
Spectrum 15	57.60	33.77	1.62	6.57	0.44

(a)

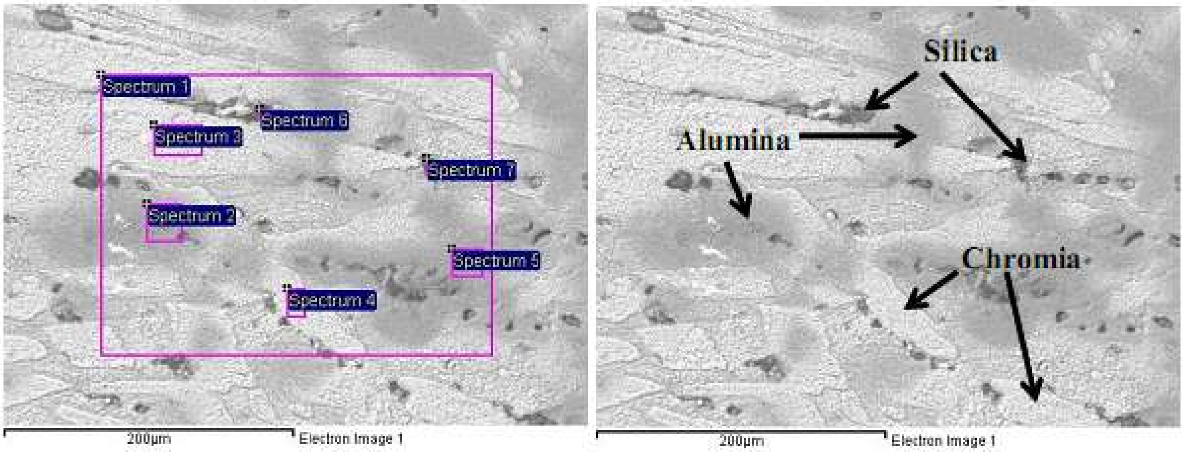
Spectrum 1
Spectrum 6
Spectrum 3
Spectrum 7
Spectrum 2
Spectrum 5
Spectrum 4
200µm
Electron Image 1
Silica
Alumina
Chromia
200µm
Electron Image 1

(b)

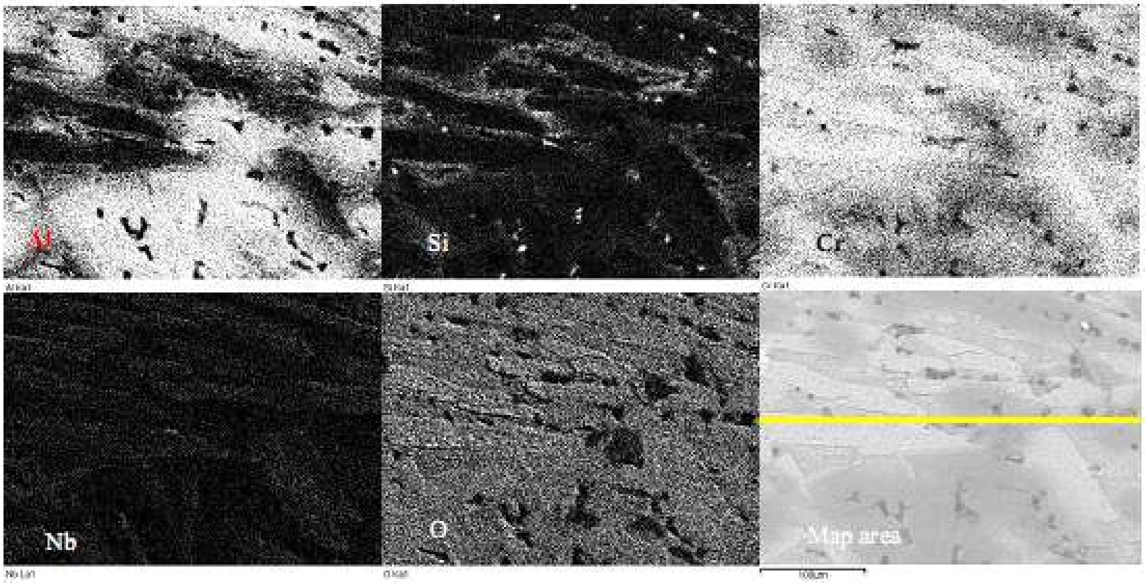
Al
Si
Cr
Nb
O
Map area
100µm

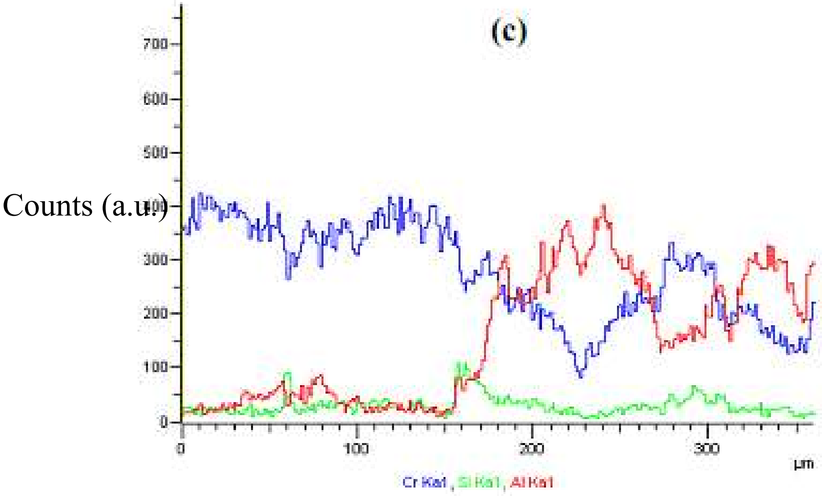

Figure 7.23 (a) Surface SEM-BSE images of oxidized AN5 specimen at 1000 °C, (b) surface elemental maps of Al, Si, Cr, Nb and O and (c) line scan of the oxidized specimen (yellow line).

decomposition of the solid solution $(Cr,Al)_2O_3$ zone and therefore the solid solution $(Cr,Al)_2O_3$ could be stable on the chromia forming constituent in the AN5 alloy. In addition, the experimental work of Sitte does not conform to the work of Besmann and is in agreement with the results of the alloy AN5. Sitte gave the Cr concentration as being equal to 24 at. % to be able to form solid solution corundum, but Besmann computed this amount to be 32 at.% [127]. The alloy AN6 had Al/Si =1 and the Al flux was enough to form continuous protective alumina scale at 1000 °C, see Table 7-10, Figure 7.13b and 7.24. The alloy exhibited parabolic oxidation behaviour for the whole exposure time with low oxidation rate constant (Table 7.4). Unlike the alloy AN5 and because of the high volume fraction of Al rich aluminide, the continuous alumina scale formed on the substrate without any Cr rich corundum. The scale mainly contained Al_2O_3 and some Cr_2O_3 and lies in the miscibility gap in the Al_2O_3-Cr_2O_3 binary system. Silica was not confirmed by the elemental map of the alloy as shown in Figure 7.24b but in the BSE image, there was a dark contrast area that contained 2 to 3 at.% Si.

(a)

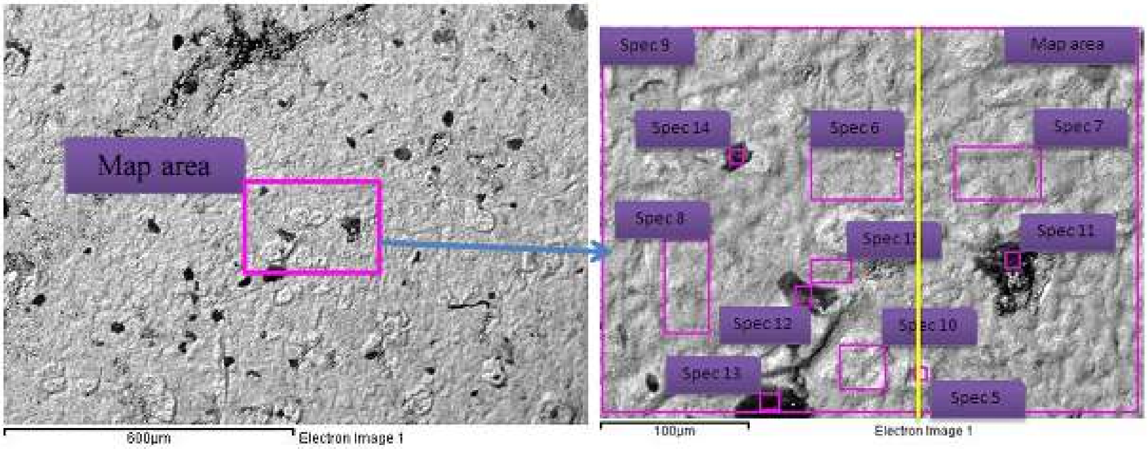
Map area
600µm
Electron Image 1
Spec 9
Map area
Spec 14
Spec 6
Spec 7
Spec 8
Spec 1
Spec 11
Spec 12
Spec 10
Spec 13
Spec 5
100µm
Electron Image 1

(b)

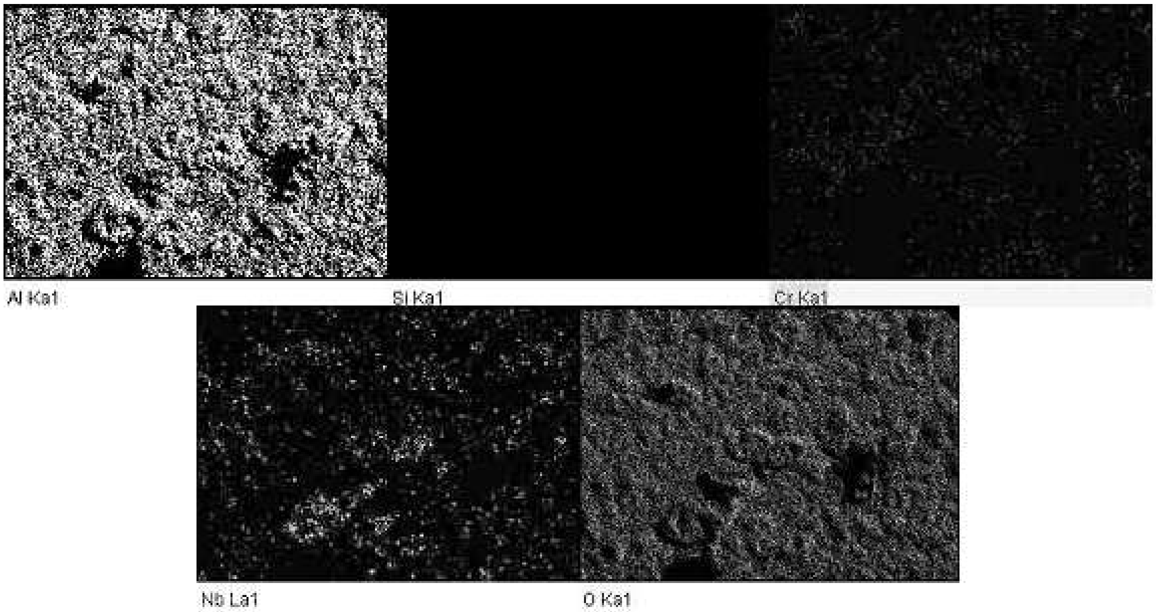
Al Ka1
Si Ka1
Cr Ka1
Nb La1
O Ka1

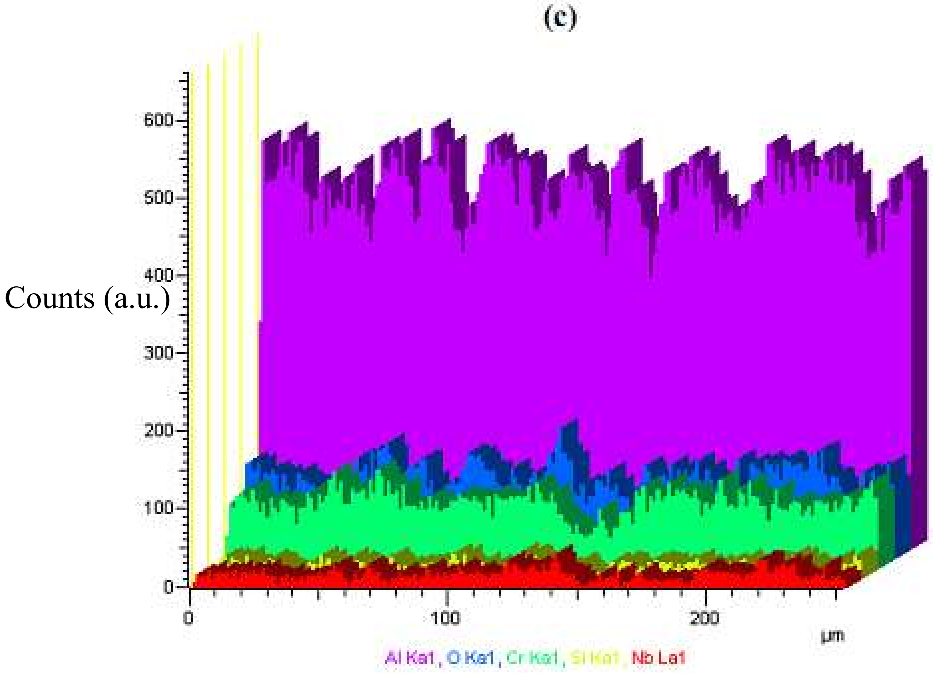

Figure 7.24 (a) Surface SEM-BSE images of oxidized specimen of AN6 at 1000 ^{o}C, (b) surface elemental maps of Al, Si, Cr, Nb and O and (c) line scan of the oxidized specimen(yellow line).

At 1200 ^{o}C the scale formed on the alloy AN5 consisted of alumina, chromia and mullite (see Figure 7.12 c and Figure 7.25 a, c). The scale was fully spalled from some faces of the cube specimen (Figure 7.25 a) and there was a continuous $(Al,Cr)_2O_3$ scale that had partially spalled from the other faces (Figure 7.25c). The quantitative EDX analyses of the scales formed on different faces (Table 7-11 and Table 7-12) would suggest that the compositions of the scale from the spalled face and partially spalled face were different. The former consisted of Al_2O_3, Cr_2O_3 and mullite and the latter consisted of solid solution corundum ($(Al,Cr)_2O_3$). According to the EDX data in Table 7-11, the Cr concentration was ~ 4.1 at. % near the surface (≤ 50 μm) from the edge of the specimen and increased to 8.3 at.% (> 50 μm) from the edge. Therefore, the increase of Cr concentration would suggest that there was volatilisation of the Cr after spallation of the alumina scale (primary scale formed on the substrate) that may cause formation of Cr_2O_3 insoluble in alumina other than forming solid solution corundum (Figure 7.12 c , Figure 7.21 a).

Table 7-11 Quantitative EDX analysis of the scale formed on the alloy AN5 at 1200 °C. The spectra are from Figure 5.25 (a)

Spectrum	O	Al	Si	Cr	Nb
Spectrum 1	52.19	40.59	3.07	4.15	-
Spectrum 2	54.88	38.57	2.43	4.12	-
Spectrum 3	54.78	38.57	2.54	4.11	-
Spectrum 4	58.02	30.73	2.52	8.33	0.40

Table 7-12 Quantitative EDX analysis of the scale formed on the alloy AN5(face 2) at 1200 °C. The spectra are from Figure 7.25 d

Spectrum	O	Al	Si	Cr	Nb
Spectrum 1	59.40	37.24	1.66	1.71	
Spectrum 2	58.23	41.28		0.49	
Spectrum 3	61.04	38.16	0.28	0.51	
Spectrum 4	58.18	41.19		0.63	
Spectrum 5	60.37	39.14		0.48	

At 1200 °C, the miscibility gap for chromia and alumina decomposition is less broad compared with that at 1000 °C (see Figure 7.21 a). Therefore, according to Besmann et al. (Figure 7.21 a), for Cr concentration between 7.2 to 24 at.%, the $(Al,Cr)_2O_3$ decomposes to alumina and chromia. The Cr concentration of the spalled surface was ~ 8.3 at.% (Figure 7.25 a and Table 7.11). This would suggest that there was decomposition of $(Al,Cr)_2O_3$ in the scale. This was not the case ≤ 50 µm from the edge. Thus, the Cr concentration was lowered to 4.1 at.% where the scale was capable of forming a solid solution corundum $(Al,Cr)_2O_3$. According to the work of Sitte, the corundum solid solution decomposes when Cr concentration is 8 to 16 at.% at 1200 °C and this is also in agreement with the results of the alloy AN5. According to the EDX data in Table 7.12, the Cr concentration on the unspalled (partially spalled face) surface (Figure 7.25 c) was between 0.48 to 1.71 at.% that lies in the $(Al,Cr)_2O_3$ solid solution stability zone with no decomposition of the oxides. This is also in agreement with Besmann & Sitte [127].

(a)

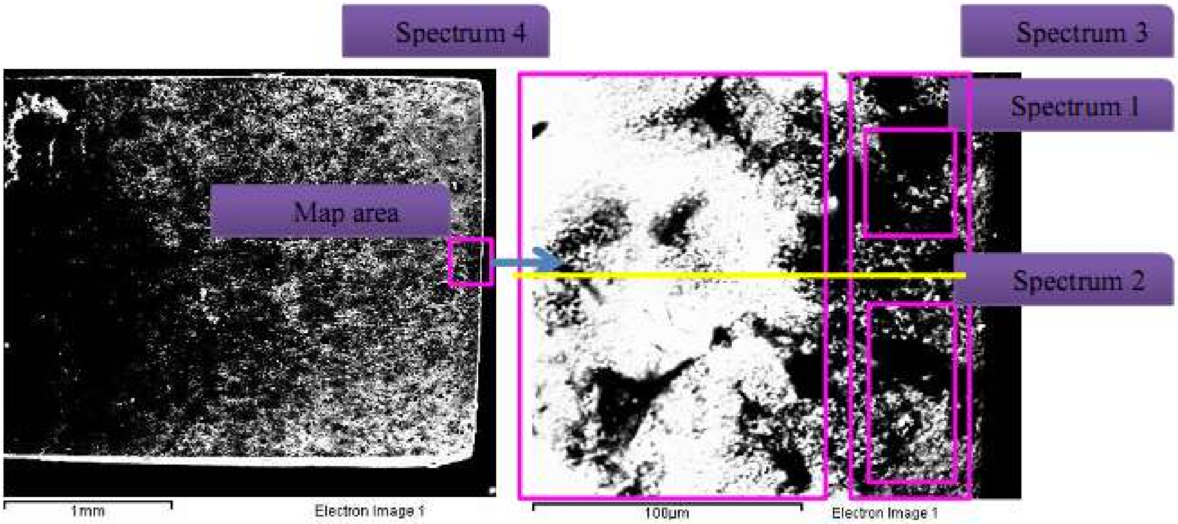
Spectrum 4
Spectrum 3
Spectrum 1
Map area
Spectrum 2
1mm
Electron Image 1
100µm
Electron Image 1

(b)

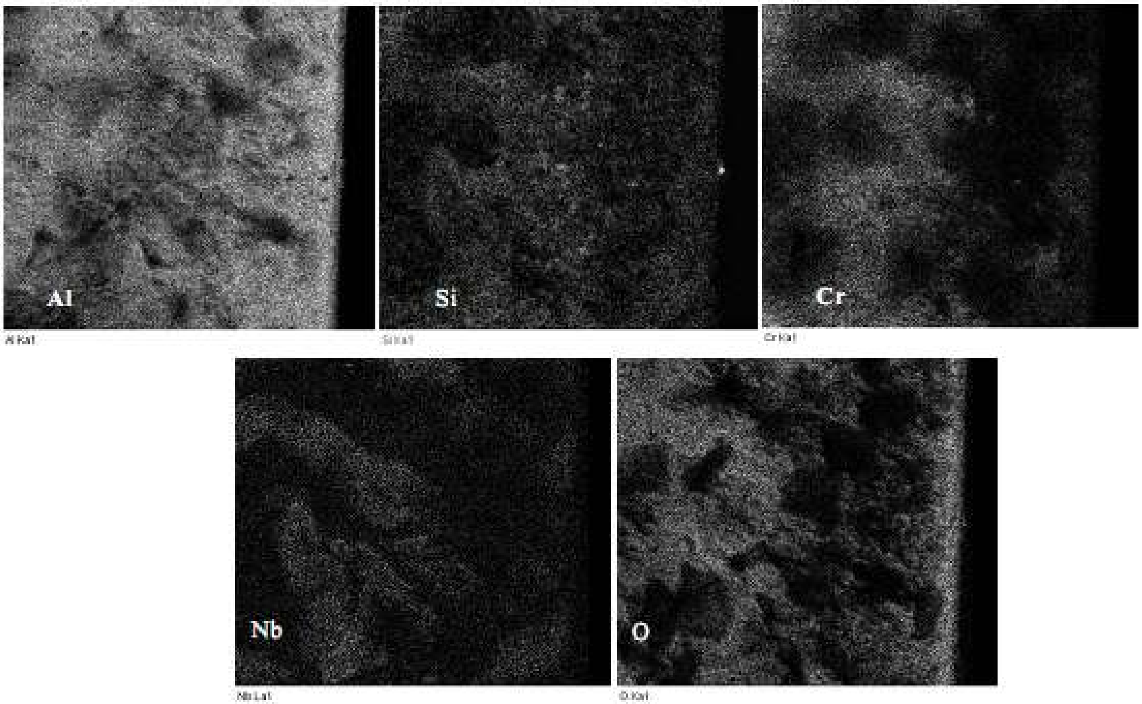
Al
Si
Cr
Al Ka1
Si Ka1
Cr Ka1
Nb
O
Nb La1
O Ka1

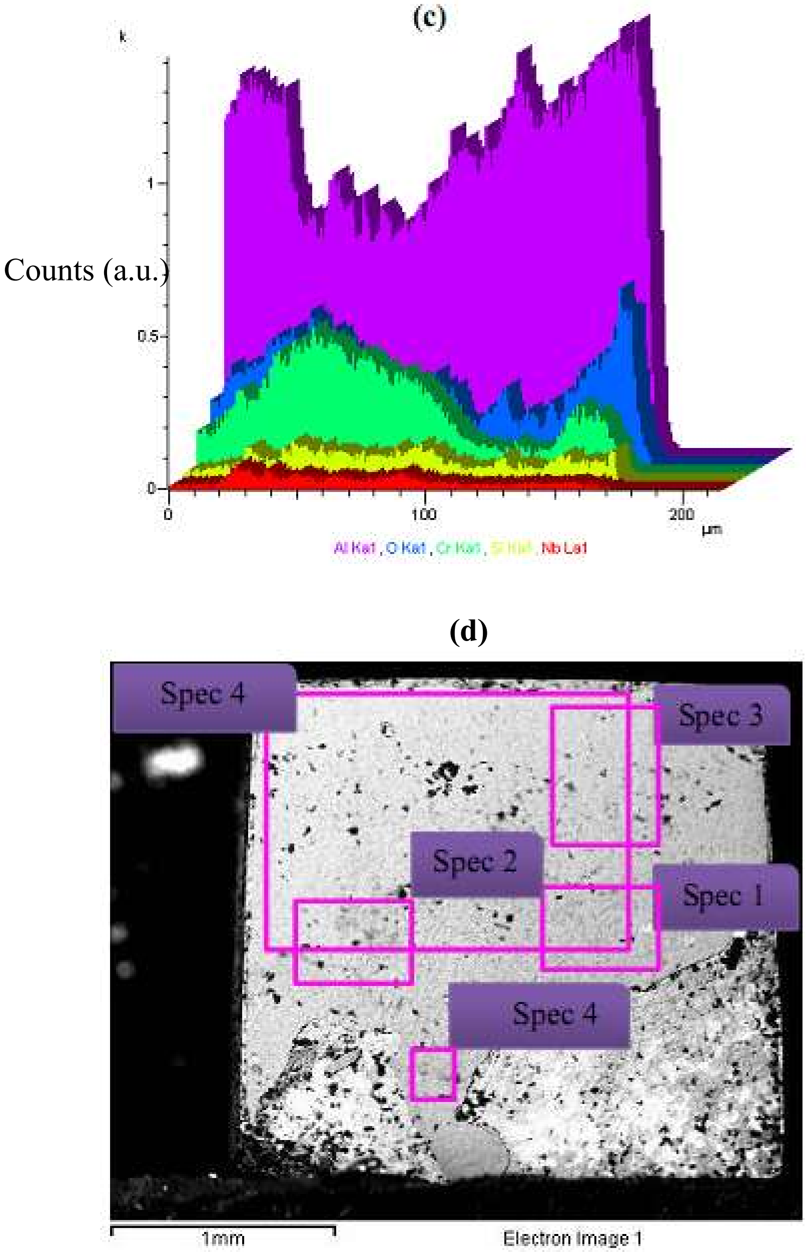

Figure 7.25 (a) Surface SEM-BSE images of oxidized specimen of AN5 at 1200 °C, (b) surface elemental maps of Al, Si, Cr, Nb and O, (c) line scan of the oxidized specimen and (d) Surface SEM-BSE images of oxidized specimen (face 2) of AN5 at 1200 °C.

The scale formed on the alloy AN6 at 1200 ^{o}C consisted of alumina, chromia, corundum with some small fraction of mullite formed in the spalled area of the ridges (Figure 7.26 a). According to the EDX data (Table 7-13), the Cr concentration in the scale was between 1.48 to 2.58 at.%. This would therefore suggest that the scale was mainly solid solution corundum $(Al,Cr)_2O_3$ and there was no formation of chromia in the scale (Figure 7.21 a). The scale was broken in some areas along the ridges owing to the internal stresses produced by scale convolution where the mullite formed (see Figure 7.26 a, b and Figure 7.13 c). The areas where the alumina scale spalled off, exhibited bright contrast, see the Si and Cr elemental maps as in Figure 7.26 b.

Table 7-13 Quantitative EDX analysis of the scale formed on the alloy AN6 at 1200 ^{o}C. This spectra are from Figure 7.26a

Spectrum	**O**	**Al**	**Si**	**Cr**
Spectrum 1	54.39	42.86	1.27	1.48
Spectrum 2	54.15	40.72	2.28	2.85

(a)

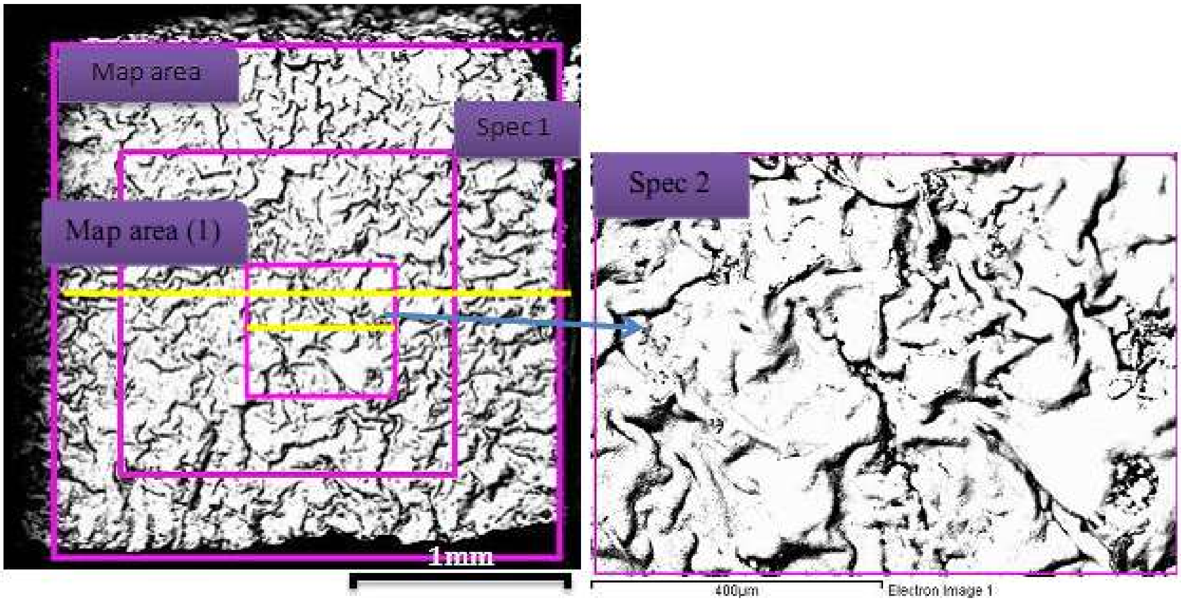
Map area
Spec 1
Spec 2
Map area (1)
1mm
400µm
Electron Image 1

(b)

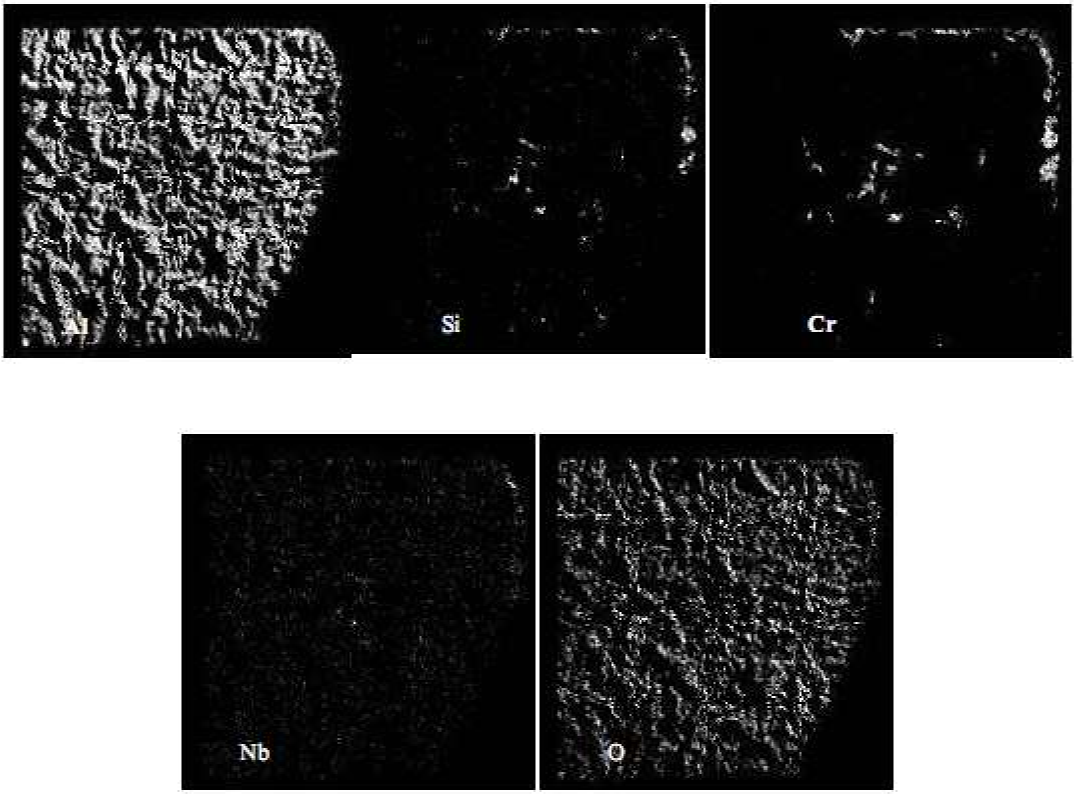
Al
Si
Cr
Nb
O

Map area (1)

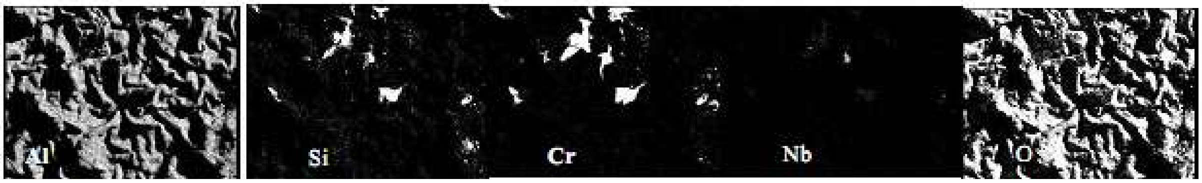

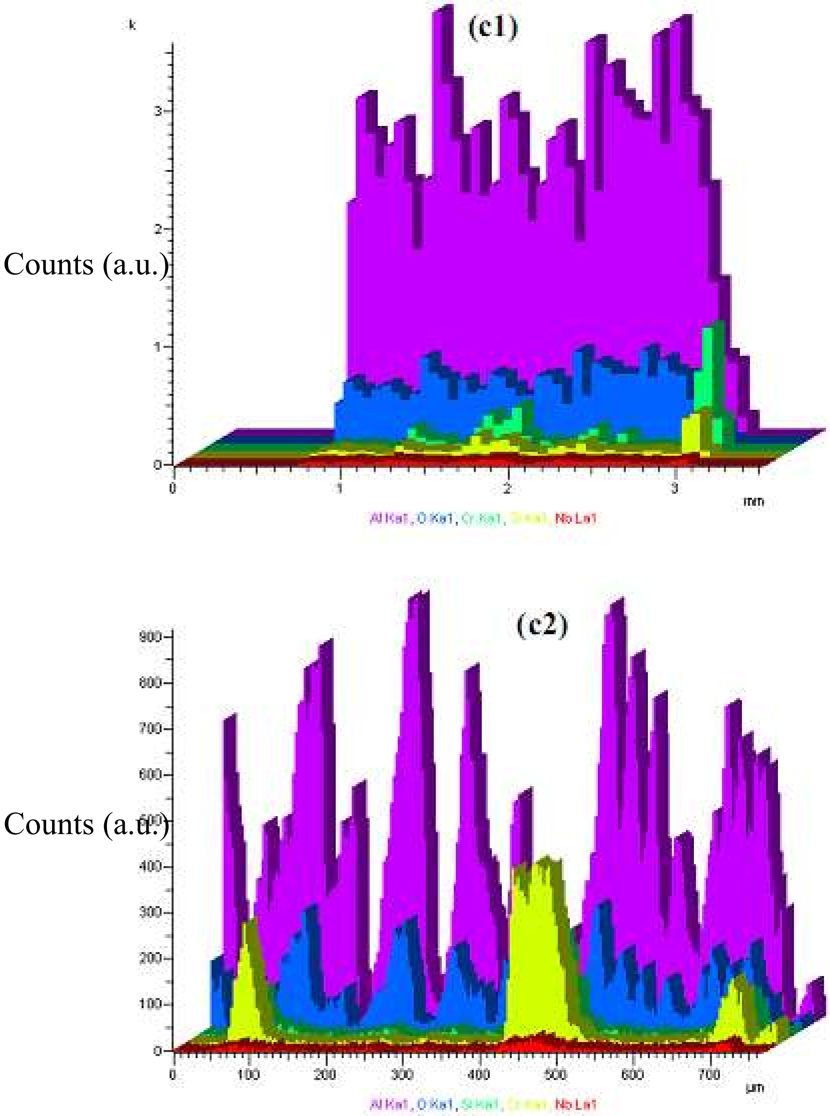

Figure 7.26 (a) Surface SEM-BSE images of oxidized specimen of AN6 at 1200 ^{o}C, (b) surface elemental maps of Al, Si, Cr, Nb and O and (c) line scans of the oxidized specimen.

Data obtained from this study is plotted together with those representing steady state growth rates from Ni, Fe, or Pt based intermetallics.

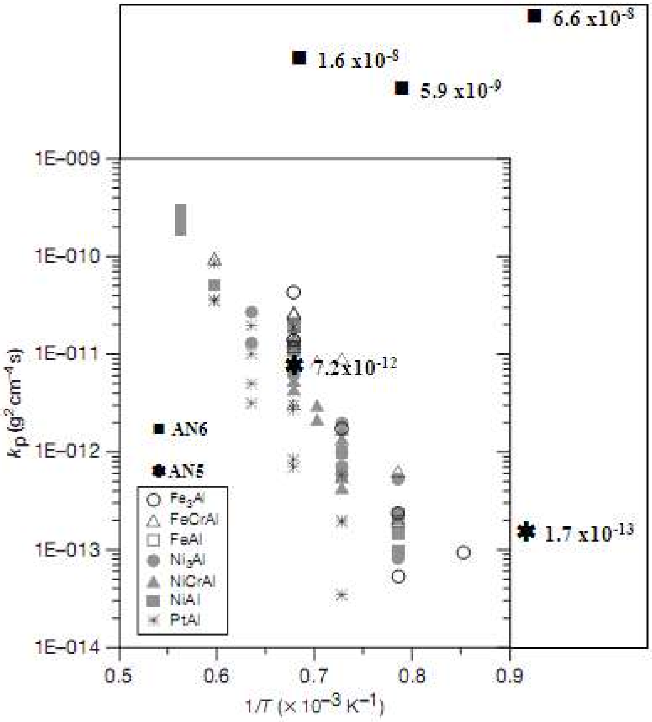

Figure 7.27 Parabolic rate constants showing the Al_2O_3 scale growth rate on different Fe, Ni, and Pt-based alloys [61]. The results of the present study are marked by bold star (AN5) and solid square (AN6).

According to the parabolic rate constants shown in Figure 7.27, the alloy AN5 lies among those intermetallics that form alumina scale following parabolic oxidation behaviour and have oxidation rate constants (kp) between $6x10^{-12}$ and $5x10^{-11}$ $g^2/cm^4.s$ at 1200 ^oC. Parabolic behaviour was not observed for the alloy AN5 for the longer exposure times and the slope of the weight gain curve versus time decreased to lower values where cubic or linear behaviour was fitted to the data. Despite of the fact that the alloy AN6 contained high volume fraction of the Al rich Al_8Cr_5 and Al_9Cr_4 phases, the alloy showed relatively poor oxidation resistance compared with the other data in Figure 7.27. It thus would be attributed to high oxygen solubility in the precursors in which there was some reactive element solubility (Nb), see Table 7-3. Indeed, regarding the ability to establish a continuous protective scale, high oxygen permeability can be highly disruptive [6]. Therefore, it is concluded that the Nb addition had a detrimental effect on the oxidation behaviour of the two alloys based on the Cr-Si-Al system whereas the Hf or Ti addition had superior effect in improving the oxidation behaviour, see chapter 5 and 6.

The oxidation rate constants of the alloys AN5 and AN6 were plotted together with chromia, silica and alumina forming alloys in Figure 7.28. At 800 °C, the alloy AN5 lies among the alumina and chromia forming alloys whereas the alloy AN6 is out of the chromia forming alloys having the worst parabolic oxidation rate constant. At 1200 °C, the alloy AN5 is in the region between the alumina and silica forming alloys in which the alloy AN6 is in the upper bound of the chromia forming alloy. The oxidation rate constant of the alloy AN5 lies between those of the M_7Si_6 and M_8Si_7 silicides.

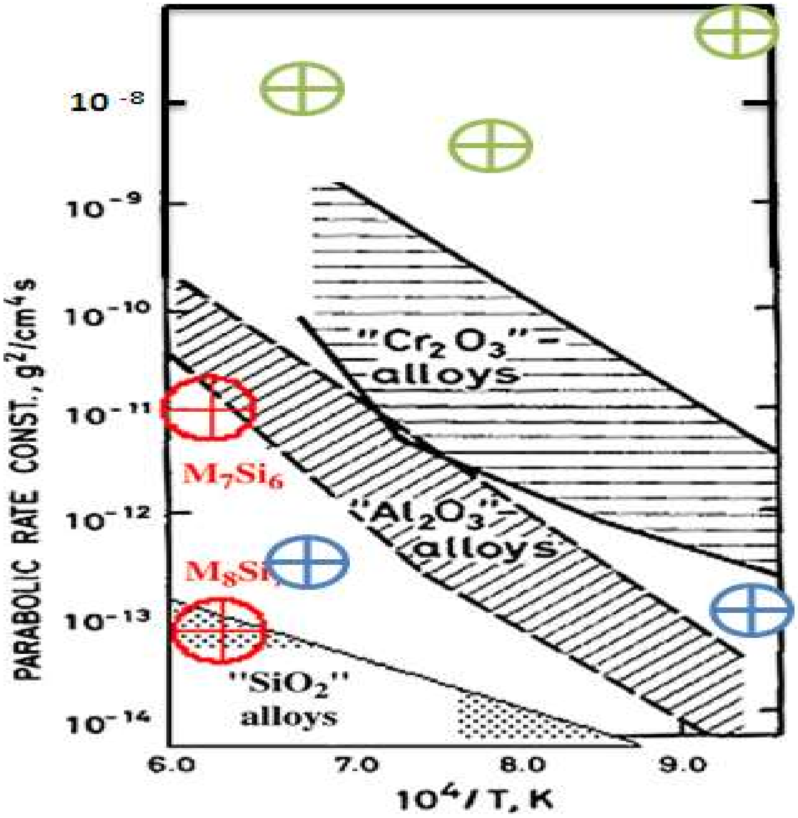

Figure 7.28 fields of kp values of chromia, silica and alumina-forming alloys. The oxidation rates of the alloys AN5 and AN6 are shown by blue and green crosses, respectively. The Red Cross shows oxidation rate of silicides studied by Zamoum et al. [103,129].

A summary of the scales formed on the alloys AN5 and AN6 is given in the Table 7-6. For isothermal exposures, it is seen that the trend with increasing temperature is from whiskers to cells to ridges or buckled scales with the exception of the alloy AN5 at 1200 °C on which a smooth scale formed without any corrugations. The alloy AN5 suffered from scale spallation that was attributed to thermal expansion mismatch between alumina and substrate or interfacial void formation. The scales grown on the alloy AN6 developed a convoluted morphology. There is a consensus that lateral growth in oxide scales is clearly indicated by scale buckling (convolutions). Another major feature is that lateral oxide growth can occur by lattice diffusion of appropriate anion and cation point defects and/or by grain boundary diffusion of one or both metal and oxygen as reactants [139].

7.4. Summary

I. Nb addition destabilized the CrSi intermetallic in the microstructure of the alloy AN5, instead stabilized the Nb_6Si_5 silicide. The microstructure of the AN5 alloy was stable after heat treatment at 1200 and 1300°C and the volume fraction of constituent in the alloy was slightly changed.

II. Nb addition destabilized the Cr_3Si phase in the microstructure of the alloy AN6, instead stabilized the Nb_6Si_5 and $Nb_{11}Si_8$ silicide. These silicides were not present in the microstructure of the heat-treated alloy at 1200 and 1300 °C. Instead, the formation of hexagonal Nb_5Si_3 along with the massive growth of Cr_5Si_3 phase observed in the alloy. There was a partial melting occurred in the alloy at 1200 °C and 1300 °C led to increase the volume fraction of Cr_5Si_3 phase. The microstructure of HT1200 alloy consisted of two different Cr_5Al_8 aluminide, one with no Nb solubility and one with 18 % Nb soluble in its lattice.

III. The Nb solubility in the Cr_5Si_3 for the alloy AN5 and AN6 is less than 1 % and there was no solubility of Nb in the $CrSi_2$.

IV. The Nb addition substantially had beneficial effect on the alloy AN5 similar to Hf and Ti, respectively, in the alloys AN1 and AN3, whereas in the alloy AN6, oxidation resistance was deteriorated in comparison to the other high-Al content alloys AN2 and AN4.

V. The alloys AN5 formed the continuous $(Al,Cr)_2O_3$ scale at 1200 °C whereas the alloy AN6 with high volume fraction of aluminide, formed a non-protective corrugated alumina scale.

VI. The poor oxidation behaviour of the alloy AN6 comparing to the AN2 and AN4 attributed to the formation of hexagonal Nb_5Si_3 in the microstructure of the alloy at the temperature range between 1000 and 1200 °C.

The evidence for alloys AN5 and AN6 would thus suggest that in the Al rich alloy AN6 with Nb addition the $CrSi_2$ is not stable while the Al_8Cr_5 is stable as well as Al_9Cr_4. The latter two phases are undesirable as they could lead to liquation in the microstructure at high temperatures according to the DSC data. Furthermore, the data for AN5 shows that with Nb as quaternary addition it is possible to form alumina in the scale up to 1200 ^oC without having a high concentration of Al in the alloy and achieve oxidation rate constant that are comparable to those of Ni and Pt based intermetallic alloys. However the increase in Al concentration of the alloy has a very negative effect on oxidation compared with Ni and Pt based alloys. The addition of Nb does reduce the solubility of Al in $CrSi_2$ like Hf does, but this phase was not destabilized by the quaternary addition of Nb in the alloy AN5 (low Al content) and is believed to play a key role in the formation of alumina scale owing to its volume fraction in the Al poor alloy AN3 which is slightly higher than in AN1. The microstructure of alloy AN5 is also desirable because the intermetallics in the Cr-Si system are expected to be exhibiting good oxidation behaviour up to about 1200 ^oC [130] compared with Al-Cr intermetallics which are expected to have good oxidation behaviour up to but not exceeding 1000 ^oC and the densities of $CrSi_2$ and Cr_5Si_3 are desirable as they are about 5 and 6.5 g/cm^3 respectively [131,132]. (the density of Cr_3Si is 6.54 g/cm^3 [131] and this phase formed in AN2 but was not stable at 1300 ^oC). In contrast with the addition of Ti in the Al poor alloy AN3 where the CrSi was stabilised at 1300 ^oC, the addition of Nb in AN5 did not stabilise the CrSi..